J Ther Eng, Vol. 11, No. 5, pp. 1392−1419, September, 2025

Journal of Thermal Engineering
Web page info: https://jten.yildiz.edu.tr
DOI: 10.14744/thermal.0000983

Research Article

Performance optimization of low-head vertical axis impulse turbine runners for nozzle angle, nozzle diameter, and nozzle standoff distance using response surface methodology

H. N. LAKDAWALA[1,*], V. K. PATEL[2], G. P. BAKHRU[3], D. N. MODI[4]

[1]*Department of Mechanical Engineering, Dr. S. & S.S. Ghandhy Government Engineering College, Surat, Gujarat, 395001, India*
[2]*Department of Mechanical Engineering,Sardar Vallabhbhai National Institute of Technology (SV NIT), Surat, Gujarat, 395007, India*
[3]*Department of Mechanical Engineering, Government Engineering College, Valsad Gujarat, 396001, India*
[4]*Department of Mechanical Engineering, University of Windsor, Windsor, Ontario, N9B 3P4, Canada*

ARTICLE INFO

Article history
Received: 27 August 2024
Accepted: 25 December 2024

Keywords:
3D Printed Buckets; Hydraulic Nozzles; Pico Hydro; Response Surface Methodology; Turgo Turbine

ABSTRACT

Pico-scale turbines, such as Turgo and Pelton, are site-specific and show variable performance under various operating and design parameters. Experimental investigation and response surface methodology were combined to optimize the geometrical parameters of Pelton and Turgo turbine runners in the present study. Low-cost, lightweight hybrid runners with 3D-printed buckets and aluminum runner discs with a vertical turbine axis were designed for low-head applications. Multivariate statistical evaluation and response surface methodology were conducted using Design Expert 13.0 software, with a central composite design applied to analyze results and optimize parameters through 80 test runs. Quadratic models describing the hydraulic efficiency characteristics of impulse turbine runners were developed via ANOVA. The study examined nozzle diameters (10-14 mm), angles (90°-95°), numbers (1 or 2), and standoff distances (40-60 mm). The optimized condition for the Turgo turbine runner was achieved with a 95° nozzle angle, 14 mm nozzle diameter, and a 40 mm standoff distance. The hydraulic efficiency of 66.19% is found, with significant model parameters having P-values below 0.0001. The findings indicated a maximum efficiency of 66.55% under optimized conditions, closely matching the proposed model with an error of 0.54%. Thus, the Turgo turbine is highly efficient and suitable for Pico hydro off-grid applications.

Cite this article as: Lakdawala HN, Patel VK, Bakhru GP, Modi DN. Performance optimization of low-head vertical axis impulse turbine runners for nozzle angle, nozzle diameter, and nozzle standoff distance using response surface methodology. J Ther Eng 2025;11(5):1392−1419.

INTRODUCTION

With a permanent magnet, a Pico turbine combines a 220V single-phase alternator with a hydraulic turbine or propeller. “Pico” denotes the power range of the alternator. Pelton waterwheel for the high heads is seated, Francis turbine is horizontal, and Run of the River Kaplan

***Corresponding author.**
*E-mail address: hnlgecs@gmail.com

This paper was recommended for publication in revised form by Assigned Editor-in-Chief Ahmet Selim Dalkilic

is a vertical Pico hydro turbine, one of the three hydraulic turbine varieties. The hydro impulse turbine is a popular, dependable, and sustainable option in hydroelectric plants, especially well-suited for moderate and high head applications. Technologies exploiting low and ultra-low head water potential sites have become popular due to their minimal environmental impact. Furthermore, putting small, creative water-related projects into action offers underdeveloped nations a cost-effective way to produce renewable energy.

A high-pressure water jet with kinetic energy is key in producing impulses. The performance of the impulse turbine suffers due to alterations in jet characteristics. The jet size and shape affect the performance of the impulse turbine. The turbine's efficiency was mainly influenced by the nozzle opening diameter or the jet diameter, speed ratio, blade count, and jet angle or the nozzle tilt angle [1]. The variability in the length-to-diameter ratio of the jet provides a method for controlling jet surface roughness over a substantial range [2]. The exact calculation of a Turgo turbine's wheel-to-nozzle diameter ratio, or D/d, is necessary since it influences wheel velocity, which influences efficiency and performance [3]. Smaller jet diameters and higher flow rates can be used to obtain the ideal operating state since the maximum brake power increases with increased discharge due to an increase in torque [4]. Higher water heads lead to increased power generation, while electric power increases linearly with nozzle diameter enlargement [5]. In descending order, the circular water jet exhibits the highest peak pressure at identical inlet pressures, followed by the common fractal shapes like square, triangular, cross-shaped, and elliptical water jets[6]. At the minimum standoff distance of the nozzle, axial flow predominates in the water jet; otherwise, radial flow is more dominant [7]. The main jet diffusion factors influencing jet quality are eccentricity-induced pressure fluctuations and jet velocity imbalance. [8]. Apart from the primary flow in the bucket, the weak secondary flows from bends or bifurcations in the Pelton turbine distributor cause minor disturbances, affecting the type of jet shape, alignment of the jet with the bucket, and shifting of the water jet core from the nozzle centerline [9]. The efficiency of Turgo and Pelton turbine runners, used in Pico hydro applications, suffers from variations in speed ratio and jet misalignment [10]. The hydrodynamically designed buckets of the Turgo impulse turbine with an optimum jet angle are required for maximum power with the best efficiency [11]. According to numerical modeling, the needle tip's position changed the velocity distribution of a Pelton turbine's free jet [12].

The variation in available head and water discharge through the turbine affects the hydraulic performance of turbine runners. In a novel way, the Turgo impulse turbine boosts a hydraulic impulse turbine's capacity while regulating flow with the nozzle and spear injector mechanism of the Pelton turbine [13]. The single-jet Turgo turbine was found to have improved performance over the baseline design, with optimized parameters by multi-criteria analysis [14,15]. Also, for a Turgo impulse turbine, the discharge plays a vital role; as the discharge increases, the specific speed rises, while with a higher net head, the specific speed decreases. Additionally, increasing the net head boosts power output [16], and reducing the water head decreases water discharge, decreasing rotational speed, torque, brake power, and efficiency [17]. The water flow rate is the only factor affecting pressure, the power produced at the alternator, and the sufficient torque applied to the shaft [18]. The Pico hydro Turgo turbine has hill charts similar to the regular turbine for low-head applications at the constant head for varying flow conditions and optimized jet angle for remote area applications [19,20]. Nowadays, researchers are attracted to the low-head operation of the Pelton runner. With a flow rate of 33 liters per minute and a static pressure head (very low) of 2.5 meters, a model of micro Pelton turbine was designed to operate at maximum efficiency using a revolutionary hydraulic system [21], and a modified Pico-sized Pelton wheel model was adapted to utilize the velocity of rainwater harvested from rooftops to supplement energy generation [22]. Micro-hydro Pelton turbines can be designed, modeled, and analyzed for remote site-specific conditions [23]. A Pelton micro hydropower turbine with a maximum head of 15 meters in rural Ethiopia could produce 32 kilowatts of electricity utilizing available water [24]. The novel design of the Turgo turbine was tested and operated with competitive geothermal efficiency to get maximum yield from steam [25]. Optimized conditions are required to operate low-head Turgo and Pelton wheel turbines for maximum hydraulic efficiency, as they are site-specific and geometry-specific [26-28].

Three-dimensional unstable flow is used to analyze flow through buckets, which is essential to the runners' performance. The fluid flow through the Turgo turbine bucket is simpler than that of the Pelton turbine. Computational Fluid Dynamics (CFD) analysis on a Pelton turbine using the RANS (Reynolds-averaged Navier-Stokes) -based Eulerian scheme predicted the complex flow patterns, jet interactions, and post-impact water interference with the buckets [29]. The instability of free surface fluid flow(sheets) in rotating buckets in three dimensions was reproduced by the study methods of the two-phase homogeneous model. [30], and with a non-orthogonal curvilinear coordinate-based boundary-fitted grid (BFG) [31], can predict the dynamic flow patterns and torque fluctuations. However, roughness on the bucket surface hinders free surface flow within the bucket, significantly impacting Pelton turbine performance and hydraulic losses, and the level of roughness magnitude influences it [32]. The bucket cutout design with the "u" type cutout and simple, improved design provides the best performance for a Pico hydro Pelton turbine [33,34]. A runner of a Pelton turbine should have the optimum number of moving buckets to operate efficiently and prevent jet interference [35]. The

enhanced hydraulic efficiency of the runner of the Turgo model can be achieved by parameterizing and numerically tuning stochastic optimization [36]. Flaws and unsuccessful designs can be detected early in the process using a 3D-printed Pelton turbine runner [37]. Coconut shell is suggested as a viable material for Turgo turbine buckets due to its robust strength and ability to endure water pressure effectively [38]. Also, buckets of the aluminum alloy, austenitic and martensitic stainless steel, and grey cast iron material have shown enough structural integrity with different bucket angles upon evaluation by numerical simulation for equivalent stress distribution and total deformation [39].

Response Surface Methodology (RSM) is a valuable tool for optimizing the turbine parameters. The Turgo turbine is effective for low-head applications (3.5 m) and can efficiently operate across various flow conditions with varying jet-to-diameter ratios. Studies have shown that RSM helps maximize energy extraction in Turgo impulse turbines, as studied by Gallego et al.[40] and for optimizing the housing basin and fluid-laden inlet channel of the gravitational water vortex hydraulic turbines by Velásquez et al. [41]. Betancour et al. [42] successfully applied RSM with the Central Composite Design technique to design a 3D-printed Gravitational Vortex Turbine (GVT) runner, with satisfactory results across a range of parameters. Guerra et al. [43] also utilized RSM to optimize the number of vanes (blades) and turbine hub-to-rotor outer diameter ratio, parameters that significantly impact the hydraulic performance of a siphon turbine. Apart from radial flow, RSM is also useful for optimizing the design of an AST (Archimedes screw turbine, an axial flow turbine) for hydrokinetic power generation applications [44]. Beyond turbine design, RSM applies to all mechanical systems to effectively optimize performance parameters. RSM has also been applied to improve heat pipes' thermal performance, as Singh et al. studied [45], and it is employed to optimize the blowdown operation of double-effect vapor absorption refrigeration systems studied by Gambhir et al.[46], and to evaluate single-effect vapor absorption systems for the dairy industry, carried out by Solanki et al.[47]. Ali[48] also demonstrated the utility of optimization for performance analysis in internal combustion spark ignition engines by adjusting low-octane gasoline with Methyl tert-butyl ether additives.

The literature review shows fewer studies on low-head vertical-axis Turgo turbines than Pelton turbine runners. Various bucket materials, such as coconut shells, aluminum, and SS 304, have been explored for their performance. However, sustainable materials like Polylactic Acid (PLA) as bucket material, combined with an aluminum runner disc, have not been reported in hybrid material runners so far. While other Response Surface Methodology (RSM) methods have been explored, the Central Composite Design (CCD) method is introduced to compare optimal operating conditions for achieving maximum hydraulic performance. Although non-dimensional numbers and ratios have been studied in past studies, the nozzle standoff distance, which considers the jet expansion effect, has not been included. This study thus bridges the gap between design and performance by optimizing most operating parameters that affect the establishment of Pico hydro off-grid power production facilities. This study is dedicated to enhancing the hydraulic efficiency of the designed runners by applying response surface methodology. It emphasizes key operational factors that play a crucial role in turbine performance, aiming to refine and improve overall functionality. The flow chart depicts the optimization methodology for the present work, as described in Figure 1.

The design of identical runners with fixed parameters is followed by manufacturing. The analysis of variance for subsequent optimization and validation tests follows the Response Surface Methodology (RSM)with a Central Composite Design(CCD).

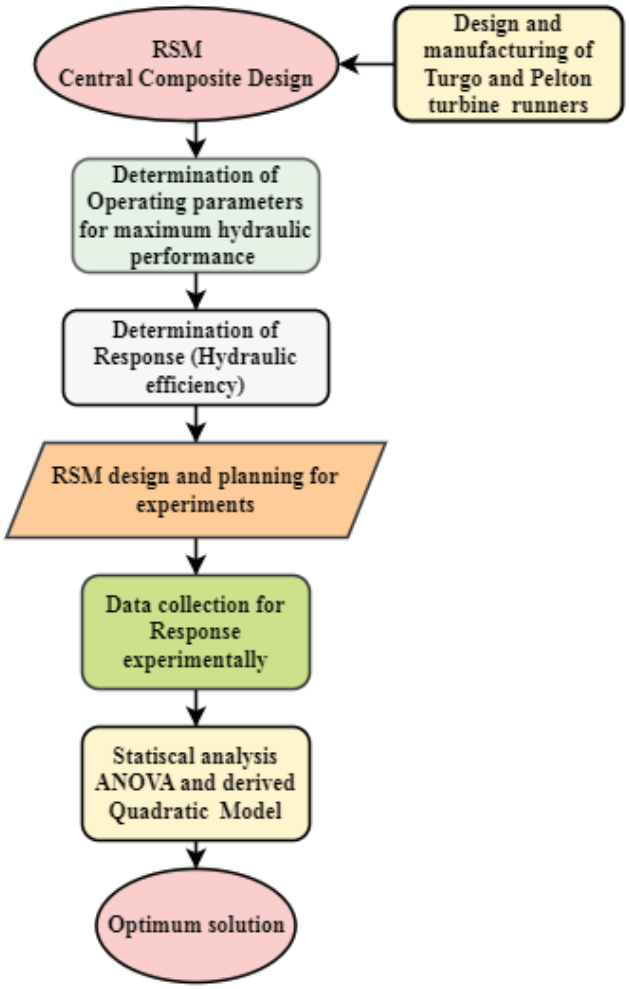

Figure 1. Flow chart for the work carried out.

The primary objective of the current experimental investigation includes

1) To study the effect of different nozzle diameters (d_j), the nozzle standoff distance (N_{sod}), number of nozzles (n), and nozzle angle (α) on the Pelton and Turgo impulse turbine runner.
2) Optimize the operating parameters for the current study using Response Surface Methodology (RSM) and Central Composite Design (CCD) to improve maximum hydraulic performance for the proposed runners.
3) To compare the optimized performance of runners with similar previous work.

METHOD AND MATERIALS

Test Configuration

The delivery line comprises 4-inch galvanized iron pipes, and a flexible hose connects to the nozzle spear mechanism assembly and header tapping. The sucked water through the collecting water sump at the water by the pump is discharged to the delivery line with a high head in an upward direction. The valve position is regulated, allowing water to flow further in the test rig. The head of 10 m is kept constant with the help of pressure gauges mounted on the header pipe. The pressure gauge measures the pressure before delivery to the flexible hose. The flow line is facilitated with overflow protection and controlled water flow.

The test rig setup is depicted in Figure 2, with all the instruments for measuring quantities using different runners and with the same pitch circle diameter (PCD), i.e., 100 mm. The turbine runners are struck with a tangentially arranged set of nozzles placed at PCD. The nozzles of 10,12, and 14 mm of aluminum have been attached to the nozzle hub. The variable flow condition is achieved with the help of the spear mechanism. The spear mechanism and the body were made from SS 304. The square acrylic frame of 1000 mm in length and width houses the vertical shaft and bearings. The runner is kept with a vertical turbine axis configuration. Also, the steel shaft has a pulley of 50 mm effective diameter fixed midway above the transparent acrylic casing to measure shaft power with absorption-type dynamometer elements connected to it. The rope, pulley, and dead weight constitute the absorption type diameter for torque measurement. The non-contact type tachometer was attached to the frame to measure runner speed. Flow measurement was achieved with the Electromagnetic type flow meter (Flowtech Digital Water Flow Meter, Model: MAG EMFM-0634, maximum process pressure 25 kg/cm^2)

Table 1. Characteristic parameters of the centrifugal pump used in the experimental setup

Description of parameter	Value
Model	Kirloskar KS-516+, Monoblock
Power rating	3.5 kW
Phase, Voltage	Three-phase, 300-400 V
Flowrate	23.7 - 13.2 LPS
Head	12-18 m
Suction lift	7.5 m
Impeller	Cast iron

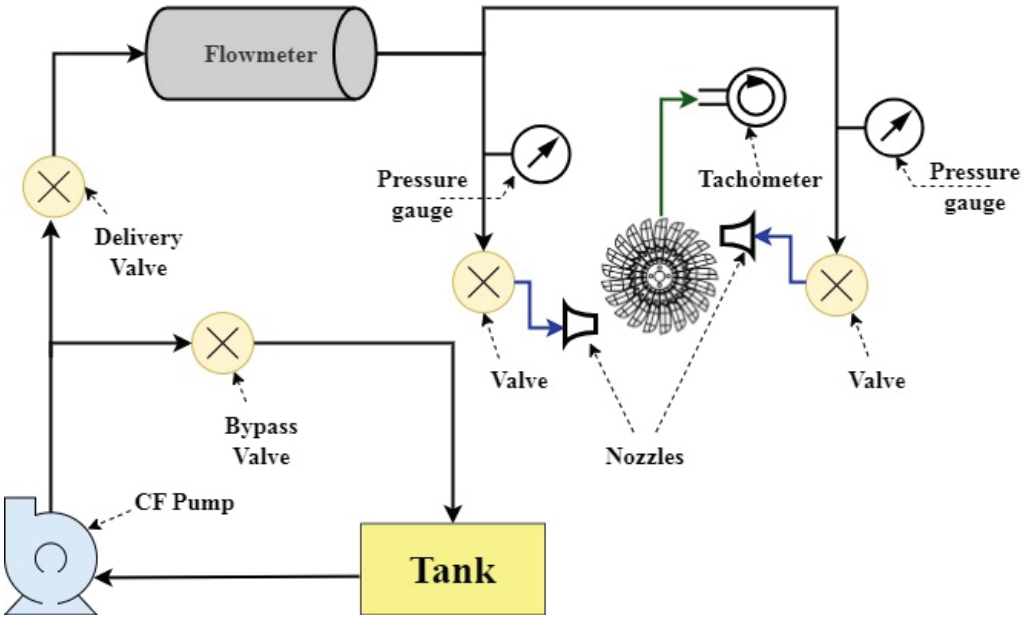

Figure 2. Line diagram for the experimental setup for testing runners with instruments measuring the process parameters.

with a measuring capacity of ±0.00069. The nozzle angle variation was set up with a protractor for each run.

The centrifugal pump attached to the bottom of the experimental setup has the following characteristic parameters depicted in Table 1. The pump has a cast iron motor body and an IP44 rating for protection. The pump has a minimum variation in efficiency over the entire operating range.

The Turgo and Pelton turbine runners were designed for experimentation. The material and specifications for the buckets and runner are depicted in Table 2 below. The runners are designed and identically sized for PCD, as mentioned in Appendix A1, and the bucket material used is the same.

The aluminum runner disc, which is 66 mm in diameter and 4 mm in thickness, has radially drilled holes for bolting buckets with 2 nos. M4 size bolts firmly, as shown in Figure 3. The runner material, aluminum, was selected for its lightweight and manufacturing ease for the present study.

The close conduit of the test setup consists of a flow measuring device, a pressure sensor, and a spear nozzle assembly at the end. An electric motor-driven impeller pump circulates the water in the entire test rig. The buckets of PTR and TTR were designed for micro Pelton turbines and suitable for Pico hydro application for a 10 m head. The buckets were designed and 3D printed using PLA material on a **Prusa i3 FDM** 3D Printer (Bed dimensions 200 x 200 x 200 mm, material layer thickness 0.05 to 0.4mm, article printing speed 20 to 200 mm/s, 3D Printer Standard Extruder

Table 2. Pelton and Turgo turbine runner with the 3D printed Polylactic Acid (PLA) bucket

Sr.No.	Bucket element	Dimensions	
		Pelton Turbine Runner (PTR)	**Turgo Turbine Runner (TTR)**
1	Bucket width (B_b) x Length (L_b)	36 mm x 34 mm	18 mm x 34 mm
2	Splitter angle (θ_s)	30°	15°
3	Hemispherical vane thickness(t_h)	2 mm	2 mm
4	Overhang length from pitch circle (L_{ov})	36 mm	36 mm
5	Notch radius (R_n)	10 mm	10 mm
6	Spherical vane outer radius (R_v)	10 mm	------
7	Overall length (L_o)	52 mm	52 mm
8	Connection bolt-hole diameter (d_h)	3.2 mm	3.2 mm
9	Aluminum runner plate diameter (D_r)	66 mm	66 mm
10	PCD of the runner (D_p)	100 mm	100 mm
11	Cutout Edge (B_c)	14 mm	------
12	Bucket Exit Angle (β_2)	15°	------

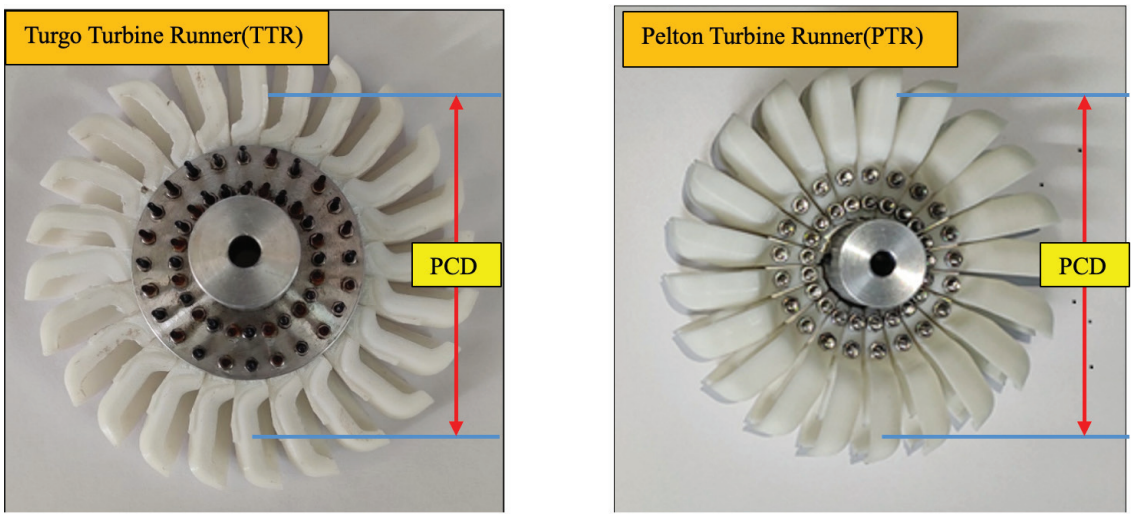

Figure 3. Designed and manufactured Turgo and Pelton turbine runners with 3D-printed buckets.

Diameter: 0.4mm, 3D Printing Software: CURA, Repetier-Host simplify3D, 3D Printing Filament Material: Polylactic Acid (PLA), Acrylonitrile Butadiene Styrene (ABS), High-Impact Polystyrene (HIPS), WOOD, Polycarbonate (PC), Poly Vinyl Chloride (PVC) and more, 3D Printing Material Diameter: 1.75mm, 3D Printing Accuracy: ± 0.1mm) manufactured by **Make3d** at the AFMFP laboratory, SV NIT Surat.

The steel vertical shaft of 15 mm diameter is stepped to 8 mm diameter for 50 mm length at one end to accommodate the runners, as shown in Figure 4. The hub of the runner accommodates the M4 grub screw to prevent relative motion between the runner and shaft. The aluminum pulley with a rope wound measured the shaft torque. The deadweight and spring balance arrangement was used to measure the rope's differential tensions and shaft power. The optimum buckets for any given PCD are about 19 to 21 because no significant flow separation at the cutout edge occurs. For the experiment, 21 buckets were selected for the Pelton and 24 buckets for the Turgo turbines. The runners' design and buckets were carried as per the micro hydro Pelton wheel turbine manual [49].

Study of Nozzle Standoff Distance and Jet Incidence Angle

The linear distance between the bucket's splitter edge and the nozzle tip is known as the "nozzle standoff distance" in PTR. On the other hand, the surface inside the bucket has a point where the jet hits in the TTR. The arrangement shown in Figure 5 depicts the jet deviation for three steps (Normal, +2.5°, and +5°. So, from normal jet incidence (perpendicular to the bucket radial axis) at 90°, it varies between 92.5 and 95 degrees in the present study.

Study of Nozzle Diameter

The aluminum nozzle hub is machined to make the dimensions shown in Figure 6(a) to reduce the spear rod assembly weight and ease machining. An orifice plate of thickness 4.77 mm acts as a nozzle with 80 degrees of divergence provided to the different concentrically drilled jet sizes.

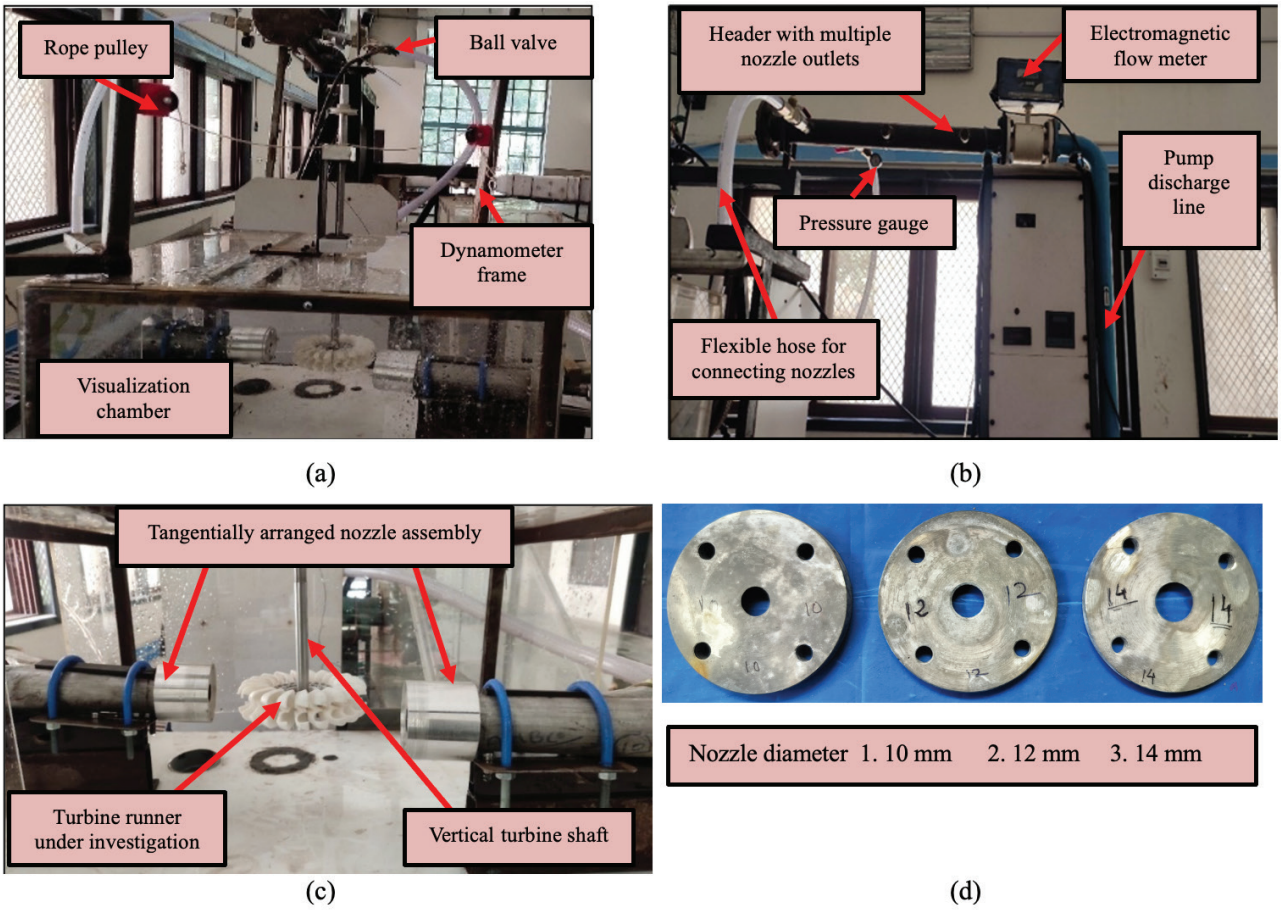

Figure 4. Experimental setup and tangential nozzle arrangement **(a)** the torque measuring arrangement, **(b)** the flow line and flow meter, **(c)** the test section-runner arrangement concerning nozzles, **(d)** the tested nozzles of diameters 10, 12, and 14 mm.

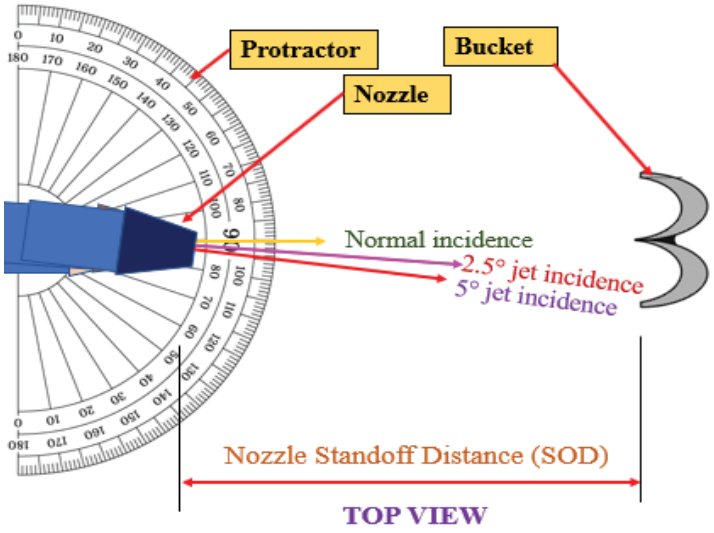

Figure 5. Concept of jet deviation (η_h) and Nozzle standoff distance (N_{sod}).

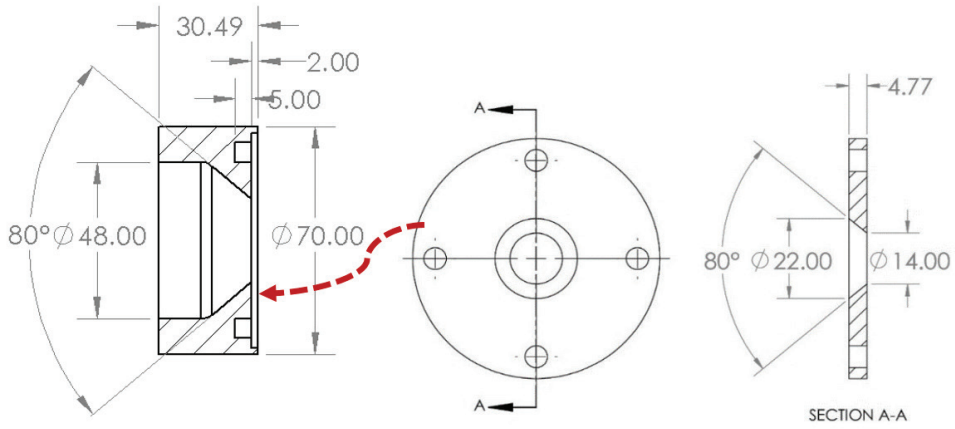

(a) (b)

Figure 6. The specifications of **(a)** Nozzle hub and **(b)** Adjustable nozzle plate.

The nozzle(jet) sizes used in the current study are 10, 12, and 14 mm, as depicted in Figure 6(b). The sitting position of the orifice plate on the nozzle hub with the help of an M4 screw is shown with the red dotted arrow. The inside threaded side of the nozzle hub can be fitted to the spear rod mechanism. The interchangeable plates of different diameters produce jets of different sizes. The standoff distance, which is typically 4 to 5 d_j between the jet exit (nozzle tip) from the spear assembly and the jet striking point on the bucket, is used.

Investigation of Hydraulic Efficiency (η_h)

The various essential variables from the study's point of view are listed below in Table 3 with operating ranges. The dimensionless quantities compare the runner's operation range under investigation. In the case of the Turgo turbine runner (TTR), a point on the bucket is considered a normal jet incidence point, and variation in angle is carried with respect to that point located from the bucket's outer edge.

The parameters shown in the above table are available for evaluation. The potential Energy provided to the turbine, or the hydraulic power to the turbine, is the product of the mass flow rate of fluid flowing through it $\dot{m}_f = \rho \times Q$ and the test-specific Energy $E_s = g \times H$. The values for range calculations are based on the direct effect on the evaluated parameter of the incurred parameter in the equations above. The data collected upon experimentation in the present study is reduced using equations mentioned in Table 4 below.

An uncertainty analysis is essential to envisage the correctness of measurements. The instruments measuring various physical quantities always suffer from inherent characteristics leading to false readings. According to the study, uncertainty was found for the head of water, angular

Table 3. Recorded input key global parameters with a range of work

Parameters	Notation	Range	
		PTR	TTR
Speed ratio (λ_s)	$= \frac{V_{jet}}{u}$	0.011-0.66	0.013-0.68
Flow ratio (ϕ_f)	$= \frac{Q}{N \times D_p^3}$	6 x 10^{-4} - 18.13 x 10^{-4}	5.4 x 10^{-4} - 10.14 x 10^{-4}
Jet ratio (ψ_j)	$= \frac{D_p}{d_j}$	6 - 10	6 - 10
Nozzle angle (α)	(α)	90-95°	90°- 95°
Energy coefficient (E_f)	$= \frac{g \times H}{N^2 \times D_p^2}$	0.0034-0.035	0.0032-0.027
Power coefficient (P_f)	$= \frac{P_d}{\rho \times N^3 \times D_p^5}$	1.16 x 10^{-8} - 7.6 x 10^{-6}	1.16 x 10^{-8} - 7.6 x 10^{-6}
Specific Speed (Ω_s)	$= \frac{\omega \times \sqrt{Q}}{(g \times H)^{\frac{3}{4}}}$	0.002 - 0.166	0.022 - 0.16
Power Specific Speed (Ω_{sp})	$= N \frac{\sqrt{\frac{P_d}{\rho}}}{(g \times H)^{\frac{5}{4}}}$	0.051 - 0.69	0.025 - 1.24
Bucket size ratio(δ_b)	$= \frac{L_b}{B_b}$	0.92	1.85

Table 4. Data Reduction

Parameters	Notation
Torque developed at the runner shaft, N-m.	$T_d = \frac{(W - S) \times D_e \times g}{2}$
Angular velocity(ω) of the runner, rad/s	$\omega = \frac{2 \times \pi \times N}{60}$
Power developed, Watt.	$P_d = T_d \times \omega$
Hydraulic power, Watt	$P_h = \rho \times g \times Q \times H$
Hydraulic efficiency (%)	$\eta_h = \frac{P_d}{P_h} \times 100$

speed, torque developed at the runner shaft, and flow rate for all the tested combinations with full gate opening (100%). Assuming volumetric η_v and mechanical efficiency η_m are approximately unity, the hydraulic efficiency is given by equation (1) as

$$\eta_h = \frac{T_d \times \omega}{\rho \times g \times Q \times H} \quad (1)$$

Since the experiments were carried out with a constant head, but considering frictional head loss and pipe fitting loss incurred to calculate the value of dH, the difference in measured and actual value of torque due to spring balance, which is taken care of by considering the most minor count. The measured value from the speed sensor and flow rate are also affected by the accuracy and subsequent error in measurement.

$$\frac{d\eta_h}{\eta_h} = \sqrt{\left(\frac{dH}{H}\right)^2 + \left(\frac{dT_d}{T_d}\right)^2 + \left(\frac{d\omega}{\omega}\right)^2 + \left(\frac{dQ}{Q}\right)^2} \quad (2)$$

According to the study, a sample calculation for uncertainty with whole gate opening (100%) and nozzle diameter, nozzle angle (Jet deviation) in the case of both a Turgo Turbine Runner (TTR) and regular Pelton turbine runner (PTR) carried out for the available head, torque, angular speed, and the flow rate was ±0.48%, ±1.03%, ±1.09%, and ±0.01% respectively as per equation (2).

Experimental Methodology

The hydraulic performance of runners is significantly influenced by the flow, speed, and energy coefficients [50],

[51]. The jet incidence angle, number of jets, and nozzle standoff distance are considered in the current study. Continuous experiments were conducted to minimize observational error and reproducibility. The experiments were conducted in a closed-circuit test facility at Advanced Fluid Mechanics and Fluid Power Laboratory, SV NIT, Surat. The maximum head available at the discharge line is 43 m, which is reduced to 10 m in a header for supplying the runner. The electromagnetic flowmeter (Flowtech MAG) is attached to the discharge line for accurate flow measurement. The spear rod mechanism at the nozzle distributes the water flow with a variable flow area by driving the spear rod in and out. As depicted in Figure 3, the water jet to the runner is supplied with either a single or two nozzles. The different jet diameters 10,12, and 14 mm were used in the present study with a 10 m head and 100 mm PCD impulse turbine runners, i.e., Turgo and Pelton turbines, in the present work. The observation was noted for the runner's speed, spring balance reading, slotted dead weight, and discharge, and processed further for analysis during each planned experimental run.

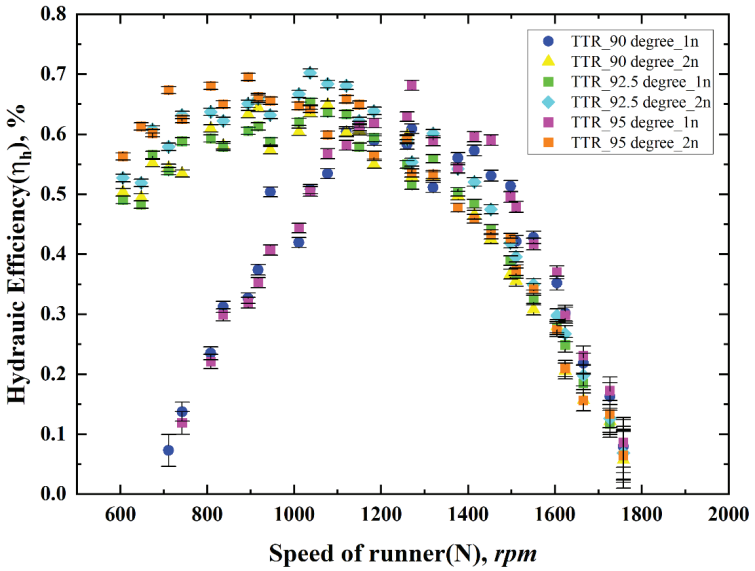

(a)

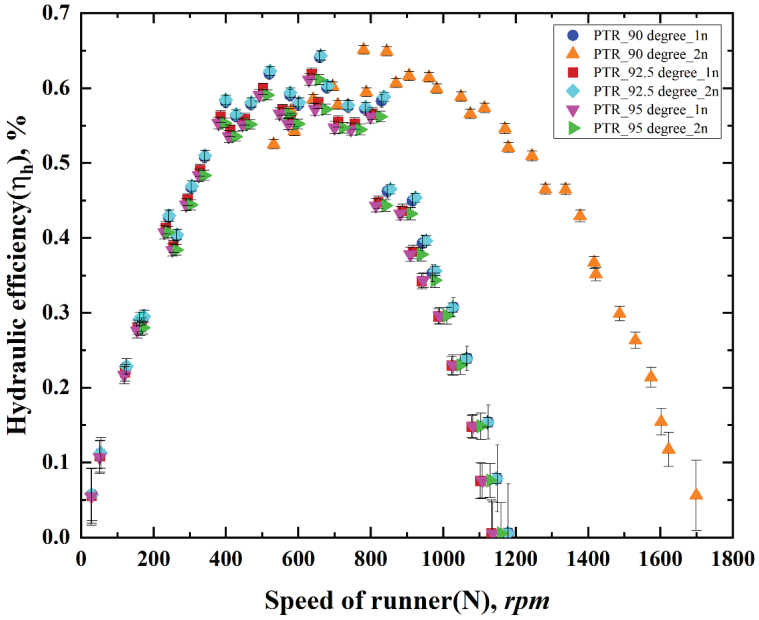

(b)

Figure 7. The performance of (a) Turgo and (b) Pelton turbine runners under variable parameters with Nozzle standoff distance (N_{sod}) = 40 mm, Nozzle diameter (d_j) =10 mm.

The experiments were carried out with all the possible combinations of parameters considered in the present study with both runners. The graph in Figure 7 depicts the PTR and TTR hydraulic performance for the 40 mm Nozzle standoff distance and 10 mm nozzle diameter. The graph has been plotted with errors evaluated by the uncertainty in the measurements of the parameters. Upon experiments and subsequent analysis, the TTR was more efficient than the PTR. It was found that the jet angle, jet diameter, and standoff distance had detrimental effects on the turbine performance. These independent parameters were taken for optimization and validation in the present work.

Response Surface Methodology (RSM)

The Response Surface Methodology (RSM) employs statistical and mathematical techniques to fit empirical data from experimental models, optimizing factors by minimizing experimental runs and analyzing factor interactions [52,53]. In the optimization process, the significance of the Response Surface lies in its function as a metamodel that encapsulates the Design of Experiments (DoE) data, enabling the formation of a rapidly executable surrogate model.

The standard RSM analyzed the performance of TTR and PTR, which were designed for Pico hydro applications. The optimization study in RSM can be performed in different stages, as described in Figure 8.

In the current study, three independent variables for the statistical experimental design: Two categorical elements, turbine runner type (PTR, TTR), and the number of nozzles (n,1 or 2) are shown in Table 5, together with three numerical factors: nozzle angle (α, degrees), nozzle diameter (d_j, mm), and nozzle standoff distance (N_{sod}, mm). These factors' levels and ranges were modified in accordance with the experimental design.

$$Y = f(X_1, X_2, X_3 \ldots\ldots X_n) \tag{3}$$

In this study, equation (3), the Y represents the experimental response, specifically hydraulic efficiency, while X_n denotes the independent variables as action factors. The regressor variables are presumed to be continuous and independent controllable within the experimental framework, with negligible errors. The aim is to replicate the true functional relationship between the response surface and the independent variables [54]. The experimental design aimed to optimize the hydraulic efficiency (as a response variable), Y. Therefore, it is crucial to establish a dependable estimation of the relationship between the independent variables and the resulting response to ensure accuracy and reliability. To reduce mistakes and the impact of uncontrollable factors, the trials were randomized and presented by equation (4).

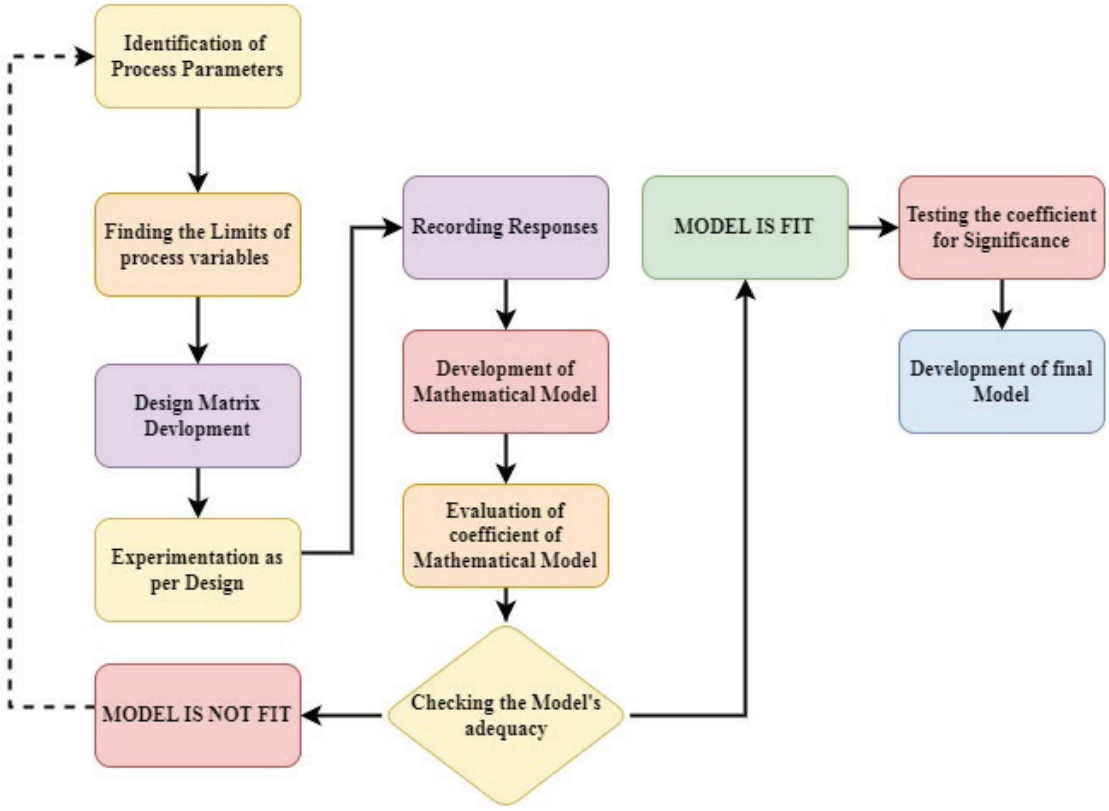

Figure 8. The flowchart for Response Surface Methodology (RSM) with Central Composite Design (CCD).

Table 5. Design of experiments (DoE), Central Composite Design (CCD) input parameters, and response

Independent variables	Notations	Factor type	Range	Coded value	Unit
Nozzle angle (degrees)	α	Numerical factor	90-95°	x_1	degrees
Nozzle diameter (mm)	d_j	Numerical factor	10-14	x_2	mm
Nozzle standoff distance (mm)	N_{sod}	Numerical factor	40-60	x_3	mm
Runner type	PTR, TTR	Categorical factor	----	x_4	----
No. of nozzles (n)	n	Categorical factor	1-2	x_5	----

Number of test runs required, $M = m_t(2^m + 2m + m_c)$ (4)

In the above equation, M is the number of required runs, and m_t is the number of categorical elements. The number of replications is denoted with m_c, while the number of numerical factors is m. So, for the present study, factorial design is 2^m composed of 3 numerical factors $2^3 = 8$; the axial section included 2m(2 x 3 = 6) points, and 3 test replications as center points are considered. Hence, it yields 80 test runs as per the above calculations. A face-centered Central Composite Design (CCD) can be achieved by selecting Alpha = 1.0; each of the five levels at which each element in the research study operates can be altered. This method reduces the complexity of implementation to three tiers for each element. With this arrangement, a quadratic model may be estimated, with the linear (first-order) terms being addressed by the 2^m factorial points and the quadratic terms being accommodated by the 2m axial points. A complete factorial design provides a simple, organized approach that thoroughly assesses the primary effects and interactions of variables.

Model And Data Analysis (ANOVA)

Equation (5) shows a second-order (quadratic) model for n parameters. In this equation, β_0 denotes the constant term, β_i signifies the linear coefficient, β_{ii} represents the quadratic coefficient, β_{ij} indicates the interaction coefficient, and ε accounts for the experimental error.

$$Y = \beta_0 + \sum_{i=1}^{n} \beta_i X_i + \sum_{i=1}^{n} \beta_{ii} X_i^2 + \sum_{i=1}^{n} \sum_{j=i+1}^{n} \beta_{ij} X_i X_j + \varepsilon \quad (5)$$

The Design Expert 13.0 software is used in this study to estimate model coefficients and conduct a statistical analysis of the experimental data. The coefficients of the developed model were determined by this program using independent data and constant variance to distributions, one-way Analysis of Variance (ANOVA). The ANOVA method was employed to evaluate the appropriateness and adequacy of the responses concerning the model's functions and variables. The models that achieved statistical significance have a P-value below 0.05. The model's statistical importance was assessed using the signal-to-noise (F value), and its validity was confirmed using the coefficient of determination (R^2). The residuals and pure errors at duplicate locations were evaluated using a lack of fit test. The formulas and processes used in the research were used to confirm the model's fit using the anticipated residual sum of squares, or PRESS.

The experiments were performed with the nozzle diameters of 10 mm, 12 mm, and 14 mm at 90° jet incidence (normal incidence), 92.5°, and 95° for both PTR and TTR. The RSM simulation–optimization method optimized the input parameters to maximize hydraulic efficiency. The CCD of RSM techniques developed a model with a standard deviation of 0.053. Regression analysis validated the model, confirming its reliability in determining input parameters for maximum hydraulic efficiency. The value of ANOVA is depicted in Table 7, corresponding to the test in Table 6, with different combinations of parameters studied under the present investigation, representing the quadratic model. The parameters considered for the present study, like nozzle angle (α), nozzle diameter (d_j), nozzle standoff distance (N_{sod}), PTR, TTR, and the number of nozzles (n), are found to affect the hydraulic efficiency (η_h) of turbine runners significantly, as experimentally.

The factor coding and the sum of squares are coded as type III – partial, respectively. The sum of squares provides the total for each variable entered last in the model. In other words, each variable's impact is assessed by considering all other variables. The significance of the model is indicated by its F-value of 90.49. An enormous F-value could only result from noise in 0.01% of cases. Significant model terms are indicated by P-values below 0.0500. Important model terms include A, B, C, D, E, AB, AC, BC, BD, CD, A^2, and C^2. If a model term's value is more than 0.1000, it is not meaningful. If the model has many superfluous terms (aside from those required to preserve hierarchy), model reduction may improve the model. The lack of fit, F-value of 0.97, indicates that the lack of fit is minimal compared to the pure error. The likelihood that noise is the cause of a significant lack of fit F-value is 54.54%. A non-significant lack of fit is preferred because the model must fit. According to Appendix A2, the proposed model in the present study is quadratic. Fitting a multivariate linear regression model with all independent variables included is the first step in the backward elimination process. The model is then refitted after the variable with the greatest p-value is eliminated. This iterative process is repeated until all of the model's remaining

Table 6. Design of Experiments (DoE) Central Composite Designs (CCD) matrix and results

Test Run (M)	Nozzle angle (α), degrees	Nozzle diameter (dj), mm	Nozzle standoff distance (Nsod), mm	C.F. 1 Runner type (PTR, TTR)	C.F. 2 Number of nozzles (n)	Results for hydraulic efficiency (ηh) Regression model		
						Exp.	Pred.	Residual
1	95	12	50	PTR	2n	0.6415	0.6383	0.0032
2	90	14	40	TTR	1n	0.6855	0.6903	-0.0048
3	90	14	60	PTR	2n	0.6755	0.6772	-0.0017
4	92.5	12	40	PTR	2n	0.6589	0.6612	-0.0023
5	92.5	12	50	TTR	2n	0.6735	0.6682	0.0053
6	90	12	50	PTR	2n	0.6795	0.6822	-0.0027
7	95	14	40	TTR	1n	0.6495	0.6458	0.0037
8	95	10	40	TTR	1n	0.6595	0.6624	-0.0029
9	92.5	10	50	TTR	1n	0.6535	0.6504	0.0031
10	90	10	60	TTR	1n	0.6695	0.6735	-0.004
11	90	10	40	TTR	2n	0.7165	0.7187	-0.0022
12	90	14	40	PTR	1n	0.6285	0.6283	0.0002
13	90	14	40	PTR	1n	0.6765	0.6711	0.0054
14	95	10	60	TTR	1n	0.6385	0.6362	0.0023
15	92.5	12	40	TTR	1n	0.6425	0.6378	0.0047
16	92.5	12	50	TTR	1n	0.6515	0.6466	0.0049
17	90	10	60	TTR	2n	0.7015	0.7006	0.0009
18	92.5	12	50	TTR	2n	0.6645	0.6682	-0.0037
19	92.5	12	50	PTR	2n	0.6525	0.649	0.0035
20	92.5	14	50	TTR	1n	0.6345	0.6372	-0.0027
21	92.5	10	50	PTR	1n	0.6315	0.6232	0.0083
22	92.5	10	50	PTR	2n	0.6435	0.6486	-0.0051
23	92.5	12	50	PTR	1n	0.6245	0.6264	-0.0019
24	90	10	40	PTR	2n	0.6815	0.6865	-0.005
25	90	14	60	TTR	2n	0.6905	0.6853	0.0052
26	95	12	50	TTR	2n	0.6545	0.6567	-0.0022
27	90	12	50	TTR	2n	0.7055	0.7024	0.0031
28	92.5	12	60	PTR	2n	0.6375	0.6455	-0.008
29	90	10	60	PTR	1n	0.6455	0.6505	-0.005
30	92.5	12	50	PTR	2n	0.6445	0.649	-0.0045
31	90	12	50	PTR	1n	0.6565	0.6572	-0.0007
32	92.5	12	50	PTR	1n	0.6215	0.6264	-0.0049
33	95	14	60	TTR	1n	0.6125	0.6117	0.0008
34	92.5	12	50	TTR	1n	0.6375	0.6466	-0.0091
35	92.5	12	50	PTR	2n	0.6585	0.649	0.0095
36	90	10	40	TTR	1n	0.6915	0.6921	-0.0006
37	95	12	50	TTR	1n	0.6365	0.6375	-0.001
38	95	14	40	PTR	2n	0.6415	0.6454	-0.0039
39	95	10	40	PTR	2n	0.6555	0.6539	0.0016
40	92.5	12	60	TTR	2n	0.6545	0.6597	-0.0052

Table 6. Design of Experiments (DoE) Central Composite Designs (CCD) matrix and results (continued)

Test Run (M)	Nozzle angle (α), degrees	Nozzle diameter (dj), mm	Nozzle standoff distance (Nsod), mm	C.F. 1 Runner type (PTR, TTR)	C.F. 2 Number of nozzles (n)	Results for hydraulic efficiency (ηh) Regression model		
						Exp.	Pred.	Residual
41	95	10	40	TTR	2n	0.6835	0.6842	-0.0007
42	92.5	12	50	PTR	2n	0.6505	0.649	0.0015
43	90	14	60	PTR	1n	0.6515	0.6547	-0.0032
44	95	10	60	TTR	2n	0.6615	0.6585	0.003
45	92.5	12	50	TTR	2n	0.6725	0.6682	0.0043
46	92.5	12	40	PTR	1n	0.6315	0.6388	-0.0073
47	92.5	12	50	PTR	1n	0.6325	0.6264	0.0061
48	92.5	12	50	PTR	1n	0.6315	0.6264	0.0051
49	95	10	60	PTR	1n	0.6125	0.615	-0.0025
50	95	14	60	TTR	2n	0.6235	0.6283	-0.0048
51	92.5	12	50	PTR	2n	0.6545	0.649	0.0055
52	92.5	14	50	TTR	2n	0.6515	0.656	-0.0045
53	95	14	40	TTR	2n	0.6655	0.6619	0.0036
54	92.5	12	50	TTR	2n	0.6615	0.6682	-0.0067
55	92.5	10	50	TTR	2n	0.6815	0.6748	0.0067
56	92.5	12	50	PTR	1n	0.6215	0.6264	-0.0049
57	92.5	12	50	PTR	2n	0.6515	0.649	0.0025
58	92.5	14	50	PTR	2n	0.6415	0.6437	-0.0022
59	90	10	60	PTR	2n	0.6835	0.6786	0.0049
60	92.5	12	50	TTR	1n	0.639	0.6466	-0.0076
61	95	14	60	PTR	1n	0.6025	0.6044	-0.0019
62	92.5	12	50	TTR	2n	0.6655	0.6682	-0.0027
63	90	14	40	TTR	2n	0.7125	0.7112	0.0013
64	92.5	12	40	TTR	1n	0.6715	0.6641	0.0074
65	90	10	40	PTR	1n	0.6655	0.6589	0.0066
66	95	10	60	PTR	2n	0.6345	0.6383	-0.0038
67	90	12	50	TTR	1n	0.6735	0.6784	-0.0049
68	95	10	40	PTR	1n	0.6255	0.6311	-0.0056
69	90	14	40	PTR	2n	0.6925	0.6929	-0.0004
70	92.5	12	50	PTR	1n	0.6315	0.6264	0.0051
71	92.5	12	40	TTR	2n	0.6915	0.6855	0.006
72	92.5	12	60	PTR	1n	0.6255	0.6226	0.0029
73	95	14	60	PTR	2n	0.6295	0.622	0.0075
74	92.5	12	50	TTR	1n	0.6435	0.6466	-0.0031
75	95	12	50	PTR	1n	0.6215	0.6181	0.0034
76	92.5	12	50	TTR	2n	0.6615	0.6682	-0.0067
77	92.5	12	50	TTR	1n	0.6515	0.6466	0.0049
78	92.5	14	50	PTR	1n	0.6185	0.6239	-0.0054
79	90	14	60	TTR	1n	0.6715	0.6638	0.0077
80	92.5	12	50	TTR	1n	0.6475	0.6466	0.0009

Table 7. Present work - ANOVA for response surface quadratic model for the hydraulic efficiency of runners

Source	SOS	df	M.S	F-value	p-value	Remarks
Model	0.0456	18	0.0025	90.49	< 0.0001	significant
A-Nozzle angle (α)	0.018	1	0.018	642.26	< 0.0001	significant
B-Nozzle diameter (d_j)	0.0008	1	0.0008	29.26	< 0.0001	significant
C-Nozzle SOD (Nsod)	0.0044	1	0.0044	157.85	< 0.0001	significant
D-Runner type PTR, TTR	0.0078	1	0.0078	278.07	< 0.0001	significant
E-No. of nozzles (n) 1n,2n	0.0098	1	0.0098	349.69	< 0.0001	significant
AB- ($\alpha \times d_j$)	0.0004	1	0.0004	15.81	0.0002	---
AC- ($\alpha \times N_{sod}$)	0.0001	1	0.0001	4.15	0.0459	---
AD - ($\alpha \times PTT / TTR$)	8.10E-06	1	8.10E-06	0.2894	0.5926	---
AE- ($\alpha \times 1n/2n$)	0.0001	1	0.0001	2.06	0.1565	---
BC- ($d_j \times N_{sod}$)	0.0001	1	0.0001	4.43	0.0394	---
BD- ($d_j \times PTT / TTR$)	0.0005	1	0.0005	17.26	0.0001	---
BE- ($d_j \times 1n/2n$)	0.0001	1	0.0001	2.9	0.0936	---
CD- ($N_{sod} \times PTT / TTR$)	0.0003	1	0.0003	9.22	0.0035	---
CE- ($N_{sod} \times 1n/2n$)	7.84E-07	1	7.84E-07	0.028	0.8676	---
DE- ($PTT / TTR \times 1n/2n$)	4.95E-06	1	4.95E-06	0.1768	0.6756	---
A^2- (α^2)	0.0014	1	0.0014	50.33	< 0.0001	---
B^2- (d_j^2)	0.0001	1	0.0001	3.1	0.0834	---
C^2- (N_{sod}^2)	0.0002	1	0.0002	7.49	0.0081	---
Residual	0.0017	61	0	--	--	---
Lack of Fit	0.0011	41	0	0.9733	0.5454	Not significant
Pure Error	0.0006	20	0	--	--	---
Cor Total	0.0473	79	--	--	--	---

*1n= Single nozzle, 2n= Double nozzle, df = Degree of freedom, SoS= Sum of squares, MS= Mean square

variables show p-values below a given threshold—typically set at 0.05.

In RSM with CCD, normal probability plots and externally studentized residuals are essential for model diagnostics and validation Figure 9(a). Figure 9(b) compares the predicted values from the model to the actual observed values for model accuracy and validation, detecting outliers and identifying patterns like non-linearity. Additionally, the internally studentized, as shown in Figure 9(c), also describes the outliers and pattern; moreover, it checks the assumption of constant variance (homoscedasticity). Also, describe the heteroscedasticity of the spread of residuals with a change in run number. Figure 9(d) shows an incorrect functional form and missing variables in the systematic pattern in the residuals.

RESULTS AND DISCUSSIONS

Measurement of Hydraulic Efficiency (η_h)

The hydraulic performance was measured by measuring various parameters like runner speed (N), flow rate through nozzles(Q), dead weight (W), and spring balance reading (S). The experimental work is carried out with varying flow conditions through the spear nozzle mechanism. An absorption-type rope brake dynamometer was used to measure the torque available on the shaft. The experiments were performed continuously for the various parameters, and different combinations of variables were considered for the present study. The results found with different configurations are given in terms of range in Table 5.

Comparison of PTR and TTR Based on Hydraulic Efficiency (η_h)

According to theoretical analysis, hydraulic efficiency (η_h) depends on parameters like flow rate, head, and fluid density. However, density remains constant for water as a fluid, so it merely depends on the remaining parameters. The runners are geometrically identical except for the bucket. The effect of independent parameters considered for the present study on the hydraulic efficiency of both runners is as follows.

Effect of Nozzle Angle (Jet Incidence Angle, α)

In the present study, the nozzle angle varied from 90 to 95 degrees in two steps of 2.5 degrees due to limitations. The normal jet incidence is desirable in the case of PTR. In

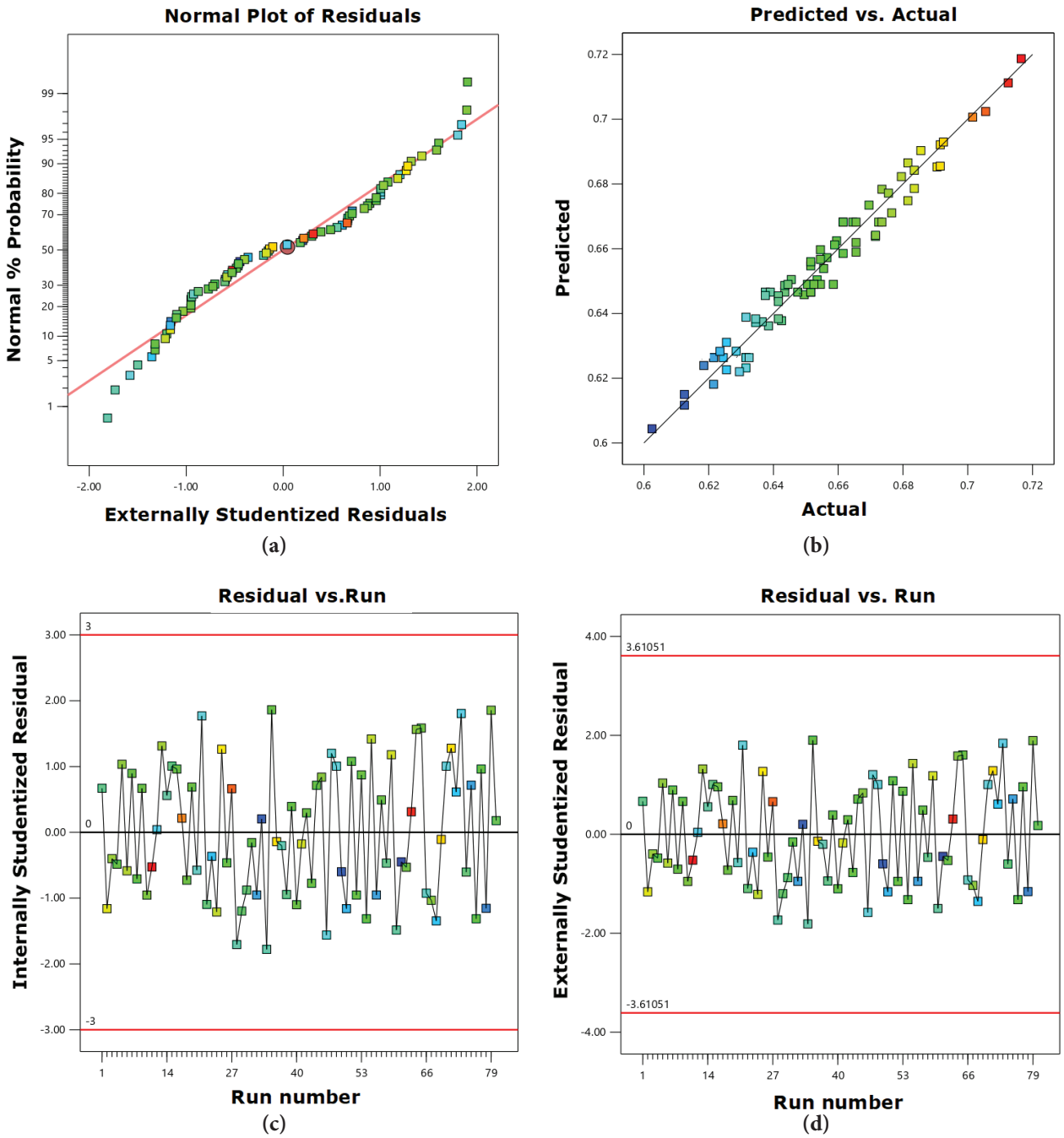

Figure 9. The graph for (a) Normal probability vs. Externally studentized residuals, (b) Predicted efficiency vs. Actual efficiency, (c) Internally studentized residual vs. Run number, and (d) Externally studentized residual vs. Run number.

contrast, TTR's hydraulic performance changes with nozzle angle variation.The larger the jet incidence angle variation from the design location, the greater the hydraulic efficiency (η_h) within a specific limit of jet incidence angle. For the present study, equations (6) to (9) revealed that the negative coefficient associated with nozzle angle tends to reduce the runner efficiency in both the runners considered here with either a single or double nozzle arrangement. The present study describes the situations where the jet misalignment contributes less to torque generation.

Effect of Nozzle Diameter (Jet Diameter, d_j)

The jet of three different sizes, 10 mm, 12 mm, and 14 mm, equal to the nozzle diameter, strikes the runner bucket in different inclinations and distances, yielding different torques on the vertical shaft attached to the runner. With an increase in jet diameter, the fluid flow rate also increases.

Conversely, the jet is more focused with a smaller diameter and more diffusion with surroundings found with a 14 mm diameter. The hydraulic efficiency (η_h) increases with a decrease in nozzle diameter(dj) in the case of PTR with a single nozzle (1n). It is found more with a double nozzle (2n), keeping the nozzle standoff distance (N_{sod}) constant but a low value of nozzle angle(α). For TTR, compared to PTR, the hydraulic efficiency (η_h) is found to be higher with low inlet angle (design point) and nozzle diameter (dj). From equations (6) and (7), the nozzle diameter (dj) is found to have a positive coefficient in the case of PTR for both single and double nozzle operations. Still, its contribution is less due to the minor terms involved than the nozzle angle(α). From equations (8) and (9), the nozzle diameter (dj) is found to have a negative coefficient in the case of TTR for both single and double nozzle operations, with less effect on hydraulic performance than the minor terms involved, such as nozzle angle(α).

Effect of Nozzle Standoff Distance (N_{sod})

For an impulse turbine, the nozzle tip distance from the runner is crucial for jet incidence. Typically, this distance is maintained between 4dj and 6dj to prevent flow separation at the jet surface. It must be optimized to avoid interference with water from the bucket. In this study, the nozzle standoff distance (N_{sod}) was varied between 40 and 60 mm in 10 mm increments. Quadratic equations (6) to (9) indicate that a 40 mm standoff distance is more effective, as it has a negative coefficient for both runners investigated. However, standoff distance(Nsod) is more negatively dominant for TTR than for PTR. The standoff distance is kept constant for the further evaluation of other parameters as attributed by RSM.

The Response Surface Methodology (RSM) with the CCD model was adopted to systematically investigate the influence of independent variables on hydraulic efficiency (η_h). This study examined three critical numerical parameters: the angle of the jet (≈ nozzle angle) (A), the diameter of the jet (≈ nozzle diameter) (B), and nozzle standoff distance (C) alongside a two categorical parameter turbine runner type (D) and number of nozzles (E), designated as independent variables. The output hydraulic efficiency (Y) was selected as the dependent variable (response).

The experimental design includes two categorical and three numerical components. To ensure the readings were repeatable, 80 experimental tests were conducted thrice, with eight test points and three replications for each category. Table 6 lists the experimental design elements and related experimental responses for the constructed model. An adequate regression model was constructed by analyzing the experimental data. An Analysis of Variance (ANOVA) was performed, a response surface model was constructed, and the Central Composite Design (CCD) responses were evaluated using "Design Expert 13.0" software. According to the different turbine types, the software determined the most important models, as explained below: Pelton Turbine Runner (PTR)-Single nozzle(1n)

$$\begin{aligned}\eta_h = {} & +0.626362 - 0.019550\times\alpha + 0.000375\times d_j \\ & - 0.008110\times N_{sod} - 0.003719\times\alpha\times d_j \\ & - 0.001906\times\alpha\times N_{sod} - 0.001969\times d_j\times N_{sod} \\ & + 0.011317\times\alpha^2 - 0.002808\times d_j^2 + 0.004367\times N_{sod}^2\end{aligned} \quad (6)$$

Pelton Turbine Runner (PTR)-Double nozzle(2n)

$$\begin{aligned}\eta_h = {} & +0.648982 - 0.021950\times\alpha + 0.002475\times d_j \\ & - 0.007830\times N_{sod} - 0.003719\times\alpha\times d_j \\ & - 0.001906\times\alpha\times N_{sod} - 0.001969\times d_j\times N_{sod} \\ & + 0.011317\times\alpha^2 - 0.002808\times d_j^2 + 0.004367\times N_{sod}^2\end{aligned} \quad (7)$$

Turgo Turbine Runner (TTR)-Single nozzle(1n)

$$\begin{aligned}\eta_h = {} & +0.646587 - 0.020450\times\alpha - 0.006575\times d_j \\ & - 0.013190\times N_{sod} - 0.003719\times\alpha\times d_j \\ & - 0.001906\times\alpha\times N_{sod} - 0.001969\times d_j\times N_{sod} \\ & + 0.011317\times\alpha^2 - 0.002808\times d_j^2 + 0.004367\times N_{sod}^2\end{aligned} \quad (8)$$

Turgo Turbine Runner (PTR)-Double nozzle(2n)

$$\begin{aligned}\eta_h = {} & +0.668212 - 0.022850\times\alpha - 0.009425\times d_j \\ & - 0.012910\times N_{sod} - 0.003719\times\alpha\times d_j \\ & - 0.001906\times\alpha\times N_{sod} - 0.001969\times d_j\times N_{sod} \\ & + 0.011317\times\alpha^2 - 0.002808\times d_j^2 + 0.004367\times N_{sod}^2\end{aligned} \quad (9)$$

A and B represent the current study's coded values for nozzle angle(α) and diameter(dj). AB denotes the interaction between these parameters, while A^2 and B^2 are the squared terms corresponding to the studied parameters. In the equations derived from the analysis, a positive coefficient indicates an increasing effect of the respective factor on the hydraulic efficiency (response) (η_h). In contrast, a negative coefficient signifies a decreasing impact. Table 7 represents the results of the ANOVA alongside the relevant statistical parameters for hydraulic efficiency (η_h).

The experimental data align well with the model's predictions, particularly when the model exhibits significant regression and an insignificant lack of fit. A strong F-value of 90.49 denotes that the model has a substantial statistical impact on the response variable. Its reliability is further reinforced by the p-value, which indicates only a 0.01% likelihood that such a high F-value could be attributed to random noise. The low error probability confirms that the proposed model effectively captures the experimental data. P-values below 0.05 indicate the significance of model

terms, while values under 0.001 indicate high importance for certain variables. Conversely, p-values exceeding 0.1 suggest that neither the model nor its components carry statistical significance. Furthermore, the model demonstrates minimal lack of fit concerning pure error, as evidenced by the lack of fit F-value of 0.9733. It is a positive outcome since the lack of fit is insignificant, indicating that the model aligns well with the predicted data.

The R^2 value, or the coefficient of determination, measures the dataset variance corresponding to the built model. In particular, R^2 is the percentage of the dependent variable's (response) variance that can be accounted for by the independent variables (predictors). An intense match between the model and the data is indicated by an R^2 value close to 1. According to Appendix A3, R^2 values greater than 0.95 indicate the model matched the data quite well, with only 0.14% of the data being unexpected. The created model's ability to predict the runners' hydraulic performance across a variety of independent variables is demonstrated by its high adjusted R^2 value. There is less than a 0.2 discrepancy between the adjusted and the predicted $R^{2,}$ having a value of 0.9532 and 0.9375, respectively. With an acceptable threshold of > 4, the correlation's suitable precision of 44.3384 indicates that the noise ratio of the model is within an acceptable range, confirming its usefulness for examining the design space. Additionally, the comparatively low coefficient of variation (0.8090) and standard deviation (0.0053) show better model validity and accuracy.

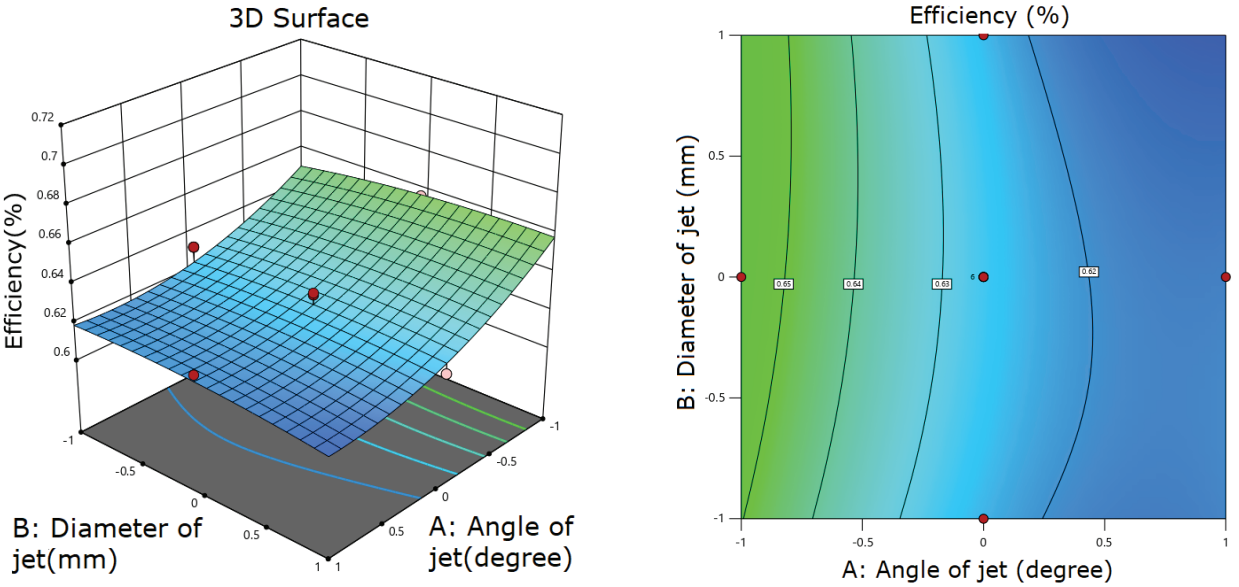

(a)

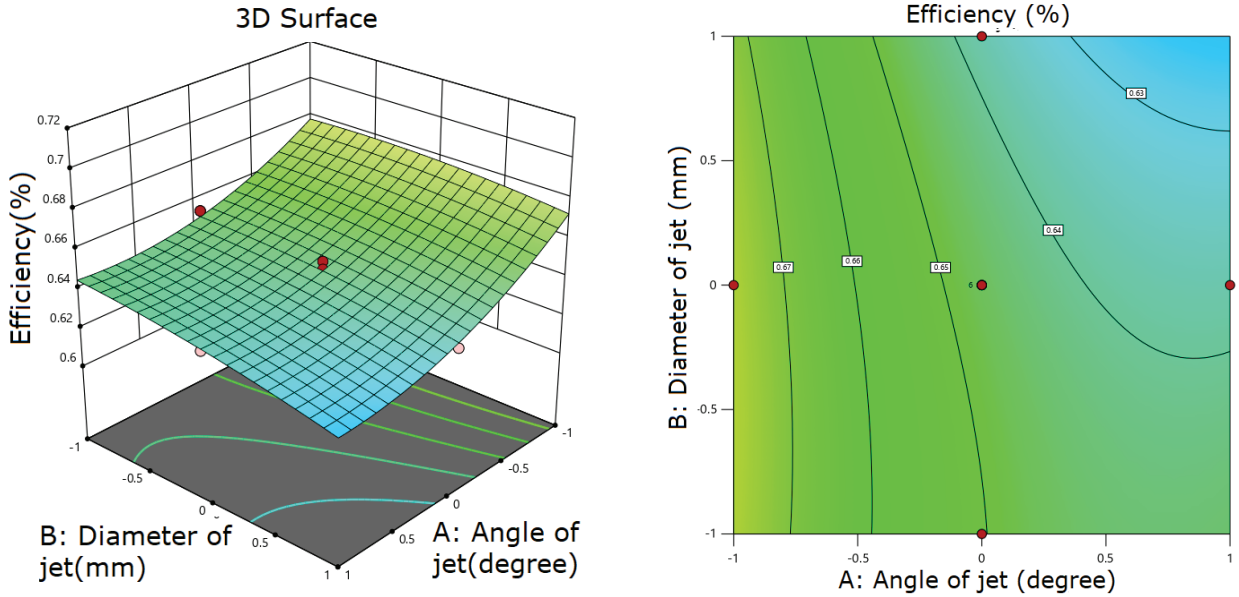

(b)

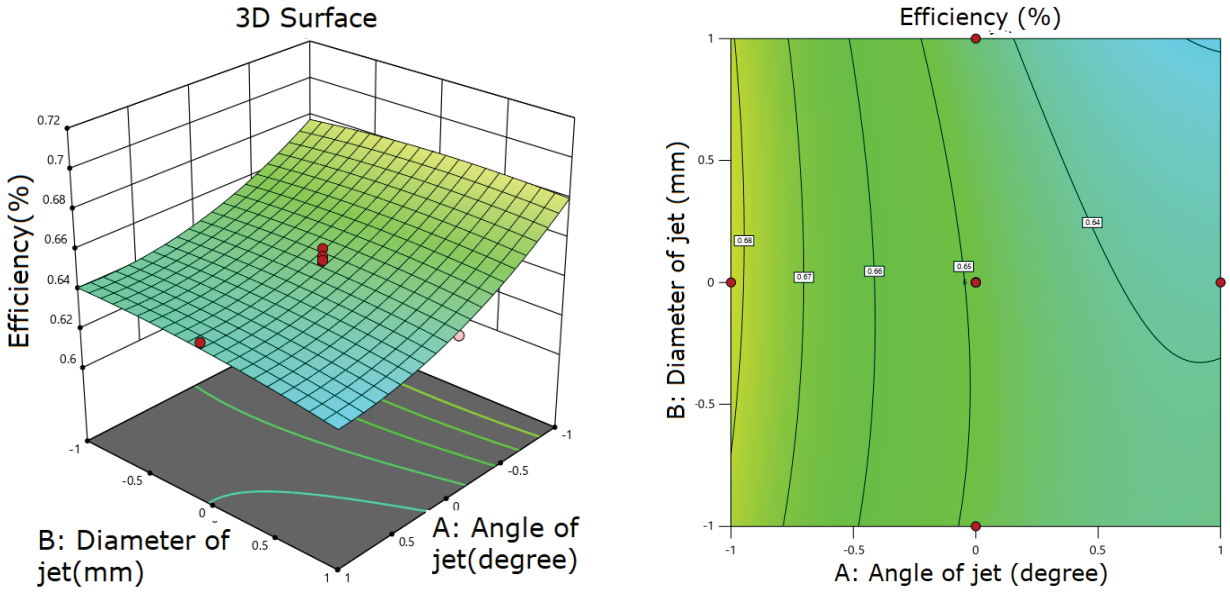

(c)

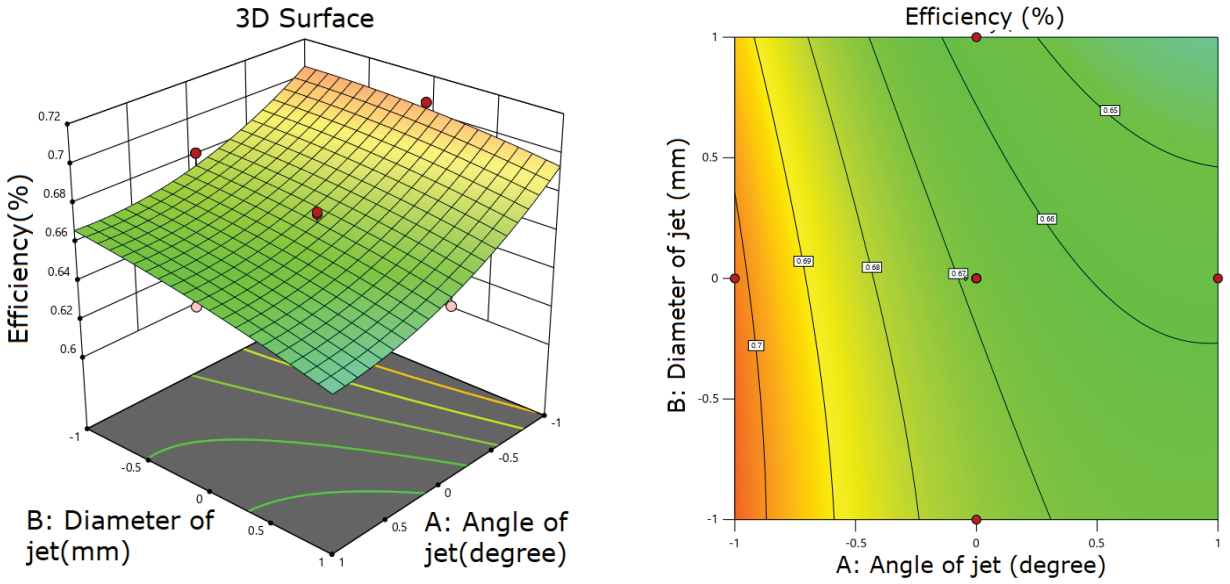

(d)

Figure 10. The response 3D surface and contour plots of hydraulic efficiency as a function of nozzle angle (α), nozzle diameter (d_j), and nozzle standoff distance (N_{sod}) in different turbine rotor types and the number of nozzles (n) of **(a)** PTR-1n, **(d)** TTR-1n, **(c)** PTR-2n, and **(d)** TTR-2n.

Table 8. Optimum values for input parameters and corresponding response

Sr. No.	Runner type	Number of nozzles (n)	Nozzle angle (α), degrees	Nozzle diameter (dj), mm	Standoff distance (Nsod), mm	Response: Hydraulic efficiency (η_h)	Goal
1	Turgo Turbine Runner (TTR)	2n	95°	14	40	66.19%	Maximization

As a result, the findings of the ANOVA analysis confirm that the developed model fits the experimental data, validating its applicability for predicting the hydraulic efficiency (η_h) of PTR and TTR with a variable number of nozzles. The evaluation of the correlational relationship between the design parameters, nozzle angle(α) and diameter(dj) versus

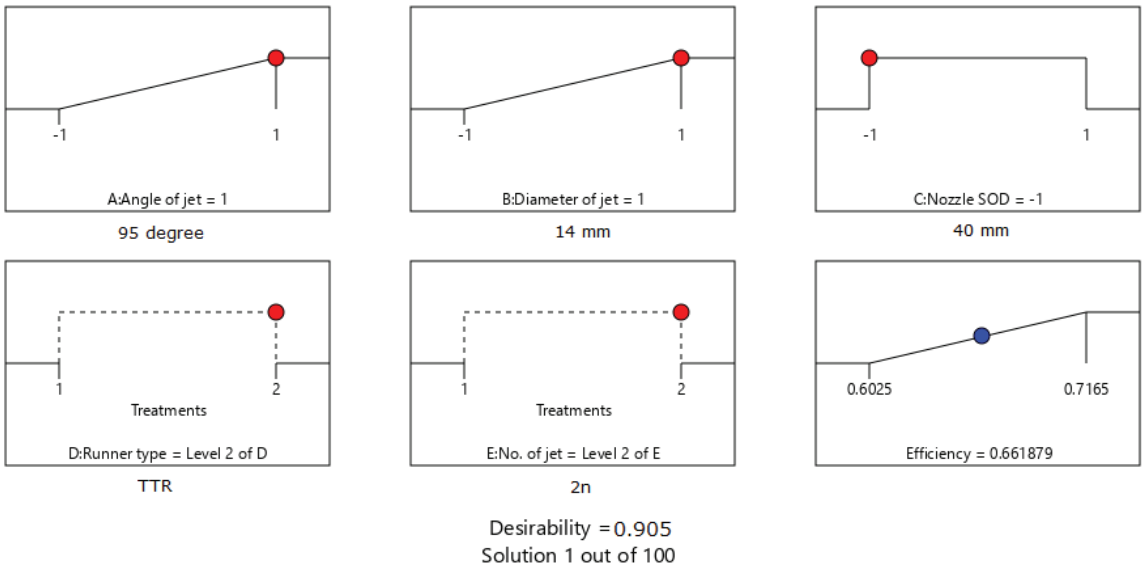

Figure 11. Desirability solution ramp for optimization of parameters for maximum hydraulic efficiency.

Table 9. Summary for comparison of present and similar past work

Sr. No.	Author/s	Parameters considered	Type of work carried out	Maximum hydraulic efficiency $(\eta_h)_{max}$
1	Alomar et al., 2022	PTR, Maximum head =110 m, Runner diameter =275 mm, nozzle diameter = 9.5 to 12.5 mm (4 nos. in equal steps), number of nozzles =1	Experimental	35.5-21.6%
2	Syofii et al., 2022	PTR, Head = 3 m, Runner diameter = 275 mm, nozzle diameter= 8 ,9, 10 mm, Number of nozzles=1	Experimental	9.01-25.44%
3	Elgammi and Hamad, 2022	PTR, Head = 2.5 m, Runner pitch circle diameter =123 mm, nozzle diameter= 9 mm, Number of nozzles=8	Experimental	10%
4	Gallego et al., 2021	TTR, Head = 42 m, Runner diameter =100 mm, nozzle diameter= 10,15,20 mm,Number of nozzles =2	Experimental & RSM with BBD model	93.7%
5	Oyebode, 2020	PTR,Head = 4 m, Runner diameter =260 mm, nozzle diameter= 51 mm, Number of nozzles=1	Experimental & statistical	-----
6	Hlabanelo et al., 2020	PTR,Head =10 m, Runner diameter =220 mm, nozzle diameter= 21 mm, Number of nozzles=2	Experimental and numerical	5-64%
7	Nigussie et al., 2017	PTR,Head = 47.5 m, Runner pitch circle diameter = 500 mm, nozzle diameter= 38.50 mm, Number of nozzles=4	Numerical	78.8%
8	Warjito et al., 2017	TTR, Head =2.7 m, Runner diameter =120 mm, nozzle diameter= 63.9 mm, Number of nozzles=1	Numerical	85.97%
9	Gaiser et al., 2016	TTR, Head =35 m, Runner pitch circle diameter =130 mm, nozzle diameter= 7.125, 12.85 and 18.59 mm, Number of nozzles=1	Experimental & RSM with CCD model	43.7-63.8%
10	Cobb and Sharp, 2013	PTR, Runner pitch circle diameter =100 mm, TTR, Runner pitch circle diameter =131 & 169 mm ,Head =17-25 m & 18- 28 m, nozzle diameter= 7.94 to 12.70 mm, Number of nozzles=1	Experimental	PTR -73% TTR- 81%-85%
11	Williamson et al., 2013	TTR, head = 0.5 – 3.5 m, runner pitch circle diameter = 150 mm, nozzle diameter =15- 35 mm (5 nos. in equal steps)	Experimental and Design of Experiments (DOE)	87%-91%
12	Present study	PTR,TTR, Head =10 m, Runner pitch circle diameter =100 mm, nozzle diameter= 10, 12 and 14 mm, Number of nozzles=2	Experimental & RSM with CCD model	For optimized conditions, Table 7

Table 10. Comparison of hydraulic efficiency η_h between experimental and RSM results for optimum values of parameters

Runner type	Number of nozzles (n)	Hydraulic efficiency η_h,%		
		Experimental results	RSM results	Error(%)
Turgo turbine runner (TTR)	2n	0.6655	0.6619	0.54

the hydraulic efficiency (η_h) for PTR and TTR is illustrated in Figure 10, utilizing contour and 3D plots generated through Response Surface Methodology (RSM). Figure 10 depicts these visualizations for the hydraulic efficiency (η_h) (response) as a function of nozzle diameter (mm), nozzle angle (α), and the nozzle standoff distance (N_{sod}), with variations in turbine runner types and also with single or two nozzle arrangements. From the 3D plots with the response contour of the hydraulic performance in Figure 10 (a), it was observed that the nozzle angle(α) significantly influences the hydraulic efficiency (η_h) for the PTR, with both low and medium values of the nozzle angle(α) yielding maximized hydraulic efficiency (η_h). Positioning a nozzle angle(α) with reference to the bucket allows the generation of adequate torque and non-interference for the bucket flow to recover before reaching the exit. Consequently, following a decrease in the hydraulic efficiency (η_h) with the high standoff distance (N_{sod}) and nozzle diameter(dj), an increase is noted in the low range of standoff distance and nozzle diameter. Figure 10 (b) presents the contour and 3D plots of the hydraulic efficiency (η_h) for the TTR single-nozzle operation. In contrast to the previous scenario, the nozzle angle(α) and nozzle diameter(dj) are more dominant than the standoff distance (N_{sod}). With an increase in the nozzle angle(α), the efficiency decreases and increases with the nozzle diameter(dj).

Figure 10 (c) illustrates the contour and 3D surface plots of the hydraulic efficiency (η_h) for PTR with double nozzles tangentially arranged at the PCD of runners. The 3D surface pattern resembles a curve for the PTR turbine type; however, this configuration harvested and converted more hydraulic Energy than the TTR single-nozzle operation. The similarities between the response surfaces for the TTR and PTR indicate a comparable effect of nozzle positioning, nozzle size, and tip distance of a nozzle under single and double nozzle on the hydraulic performance of the runner. The contour plot and three-dimensional response surface illustrating the hydraulic efficiency (η_h) for the TTR with double nozzle (2n) are presented in Figure 10 (d). This visualization demonstrates that the amount of Energy extracted efficiently by the runner is superior to that of alternative turbine runner types, with a notable finding that reducing the nozzle standoff distance (N_{sod}) leads to increased hydraulic efficiency (η_h). The contour plots and 3D response surfaces shown in Figure 10(a, b, c, and d) further emphasize the significant correlation between nozzle angle(α) and nozzle diameter (dj).

Moreover, the interaction analysis between nozzle standoff distance (N_{sod}) and hydraulic efficiency (η_h) also indicates that variations in the number of nozzles(n) notably influence hydraulic efficiency (η_h). These findings suggest that alterations in the nozzle angle(α) exert a more pronounced impact on the hydraulic efficiency (η_h) of TTR than changes in nozzle diameter(dj) and nozzle standoff distance (N_{sod}), with lower hydraulic efficiency (η_h) achieved at lower nozzle diameter(dj), nozzle standoff distance (N_{sod}) and single nozzle (1n). Overall, by optimizing the nozzle angle(α), nozzle diameter(dj), nozzle standoff distance (N_{sod}), and the number of nozzles(n)for the two runners, it is feasible to enhance the hydraulic efficiency (η_h) of the PTR by up to 10% and TTR by up to 13%.

The study utilizing Response Surface Methodology (RSM) yielded several key findings regarding the influence of independent variables on the output, which is considered the hydraulic efficiency (η_h) of the turbine runner for Pico hydro application. It was determined that nozzle angle (A), nozzle diameter (B), nozzle standoff distance (C), and the number of nozzles (E) significantly affect the hydraulic efficiency (Y) of both the runners (D), with specific combinations of these variables identified as optimal for maximizing efficiency. The regression model developed from the experimental data demonstrated a robust fit and predictive capability. It was validated through ANOVA, which highlighted the statistical significance of both the types of factors and their interactions. The response surface plots provided a visual representation of these interactions, indicating how variations in one parameter can influence hydraulic efficiency in conjunction with others. Furthermore, the findings have practical implications for turbine operation and design, suggesting that strategic adjustments to nozzle angle(α), nozzle diameter(dj), nozzle standoff distance (N_{sod}), and the number of nozzles (n), alongside careful consideration of turbine runner type, can enhance performance. Lastly, the study recommends avenues for future research, including further exploring additional variables like debris and fluid density, as it is to be used for Pico hydro off-grid applications and turbine configurations to refine the understanding of their impacts on hydraulic performance.

The TTR has a half bucket compared to the PTR and a much better tendency to accommodate a higher flow rate with a half bucket width. The speed of TTR was found to be higher compared to PTR. One of the objectives was to find the optimal hydraulic efficiency as a response to the

allied design parameters. The values found in the current study for the range of parameters investigated are shown in Figure 11 for the quadratic model with red and blue balls on the graph. It has been observed that the optimal values of the numerical parameters, nozzle angle(α), nozzle diameter(dj), and nozzle standoff distance (N_{sod}), are within the range and around the model's highest expectation.. The condition of optimality for TTR is depicted in Table 8 below. The solution is found with the objective of maximum hydraulic efficiency under given head and variable flow rate conditions. For validating the model, desirability is close to 1, and in the present study, it is found to be about 0.905, which shows good agreement between output and the desired output.

The optimum value of hydraulic efficiency achieved to maximize the hydraulic efficiency was found when the double nozzle configuration had a 40 mm nozzle standoff distance, nozzle angle, and nozzle diameter of 95° and 14, respectively.

Optimum Conditions for Maximum Hydraulic Efficiency $(\eta_h)_{max}$

The main objective of this investigation is to identify the maximum hydraulic efficiency by determining the operating and geometrical parameters that facilitate the most efficient operation of the system. The designed parameters and the required model responses for the optimization process are comprehensively detailed in Table 8. This table specifies that the response hydraulic efficiency (η_h) is integral to the optimization efforts. The input parameters were constrained within predetermined ranges to maximize the identified response. Under these conditions, the TTR achieved the maximum hydraulic efficiency of 66.19% (as illustrated in Table 8 and Figure 11). For TTR, it corresponds to a 95° nozzle angle,14 mm nozzle diameter, a 40 mm standoff distance, and the PTR turbine type with double nozzle (2n). The experiment, RSM-based input parameter optimization work, and the corresponding responses in hydraulic efficiency (η_h) carried out by various researchers are highlighted in Table 9 for comparison. The variation in maximum hydraulic efficiency $(\eta_h)_{max}$ in the last column is a relative term, as the variation in geometrical and operating parameters of the turbine runner is considered for research.

The current research found that the hydraulic efficiency (η_h) for TTR was significantly higher than previously reported findings(Sr No.6, Table 9). It is also noted that most of the past work tabulated is done on horizontal axis turbine runners, unlike the vertical axis considered in the present study. This research shows that jet diameter, angle, and nozzle standoff distance significantly improve impulse turbine hydraulic efficiency (η_h). On the other hand, for Pico hydro applications, the RSM optimization method can enhance the vertical axis TTR's performance. When considering the PTR double nozzle configuration, the TTR configuration yielded a higher gain in hydraulic efficiency(η_h). However, there isn't a recognized way to compare the abilities of various hydroturbine runners. This study developed an RSM model for impulse turbine runners to achieve these objectives.

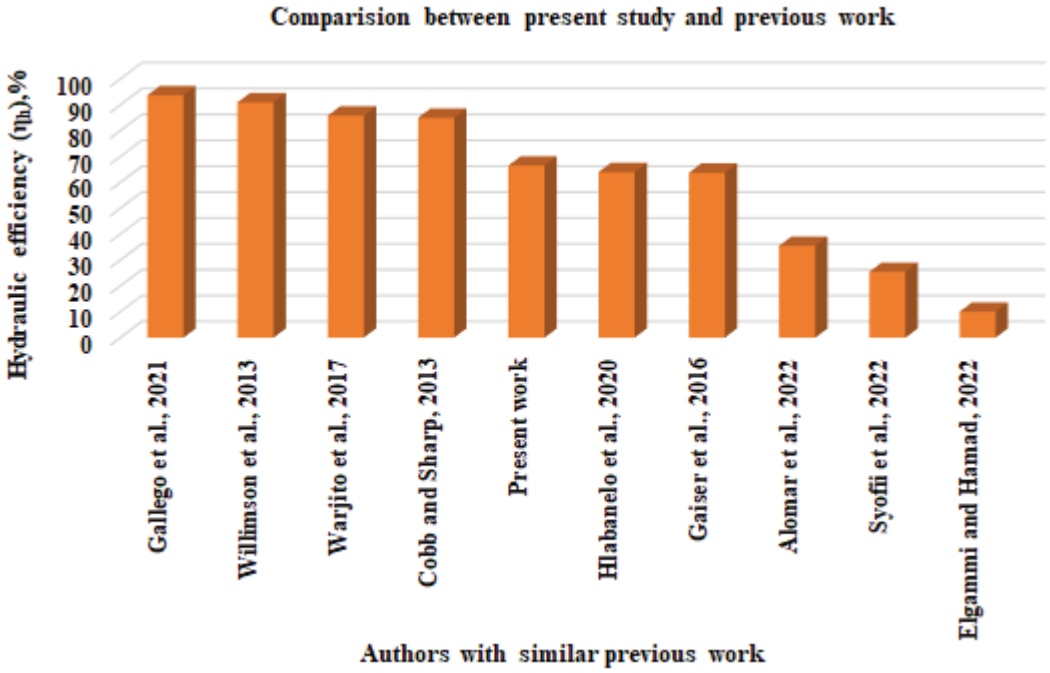

Figure 12. Comparison between similar previous work and the present study for maximum hydraulic efficiency.

The RSM model's output is compared with experimental data to validate the ideal conditions for the anticipated parameters, as Table 10 illustrates. Excellent agreement between the experimental data and the suggested RSM model is demonstrated by the results of the confirmation test, which show a slight discrepancy (0.54%) between the predicted and real hydraulic efficiency (η_h). The results of the present investigations have been compared with similar previous work on a bar chart for maximum hydraulic efficiency. Figure 12 shows that the present study yielded hydraulic efficiency under optimized conditions under a head of 10 m compared to a lower runner PCD of 100 mm in earlier studies. The comparison revealed higher efficiency bars in the previous work due to increased head, number of nozzles, nozzle diameter, runner type, or runner diameter.

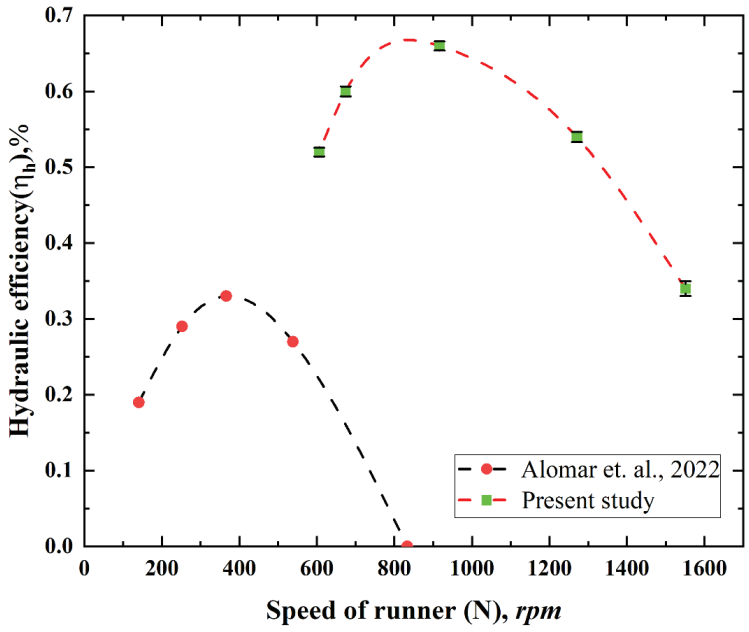

(a)

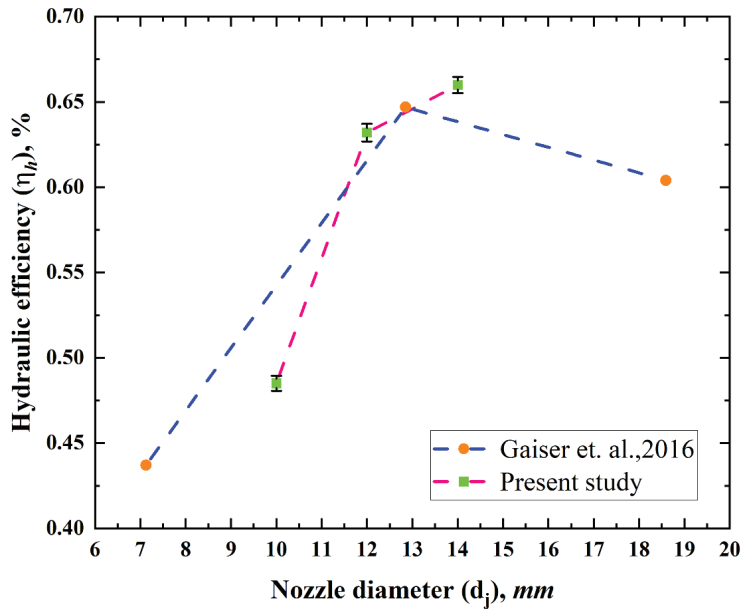

(b)

Figure 13. Turbine runner with a hydraulic performance comparison between similar previous and the present work findings (a) based on runner speed (b) based on nozzle diameter

The hydraulic performance of the PTR in the present investigation has been compared with similar previous work carried out by Alomar et al. in 2022, which had a 110 m head and 10.5 mm nozzle diameter. The trendline for the present work has been shown with error bars for the 10 mm nozzle diameter, 40 mm nozzle standoff distance, and double nozzle arrangement in Figure 13 (a). The trend lines match, and it has been found that the 65% hydraulic efficiency in the present study is higher than 33.3% of the parameters studied compared to those reported by authors in their previous work. The nozzle diameters are also checked for the findings obtained in the present study, as depicted in Figure 13 (b) in the case of TTR. The TTR in the present study is compared with the TTR for a similar trend reported by Gaiser et al. in 2016, with a head of 35 m, a runner pitch circle diameter of 130 mm, and a single nozzle. The highest efficiency observed in their study was 64.7% with a 12.85 mm nozzle.

In their work, the head, runner diameter, and flow rate are more than those investigated in the current study. However, the current curve with 100 mm PCD,14 mm nozzle diameter, and 10 m head follows the same trendline. So, the present study has the least value of parameters, with the increased value of the hydraulic performance for the runners investigated. Thus, it suggests improved hydraulic efficiency with optimized parameters.

It has been found that the vertical axis turbines investigated in the present study are more suitable for low head conditions for the given set of design and operating parameters considered. It indicates that the present study is suitable for installing off-grid Pico hydro applications for power generation in remote areas.

CONCLUSIONS

This study aimed to assess the performance of developed impulse turbines (PTR and TTR) running at optimal efficiency levels using response surface methodology (RSM)with central composite design (CCD). The experimental test was conducted to optimize the range of operating parameters, viz. jet incidence angle(90°-95°), nozzle diameter(10-14 mm), and number of nozzles(1 or 2) at a standoff distance(40-60 mm) under low-head operation(10 m) for the range of global parameters. The hydraulic efficiency assessment of the Pelton and Turgo turbines was compared at optimum conditions, and the following conclusions were made.

- It has been found from the literature studied and cited here that multiple research studies have been conducted in the past with horizontal axis low-head Turgo and Pelton turbines, and the vertical axis with jet deviation(α) is sidelined. Also, the effect of nozzle standoff distance (N_{sod}), which affects hydraulic efficiency (η_h) due to jet expansion, has not been identified or studied.
- The Polylactic Acid (PLA) for 3D printed buckets with aluminum runner discs was a low-cost solution compared to metallic bucket material for power generation at low head.
- With a standoff distance of more than $4d_j$, the jet deviates due to diffusion in the surrounding environment, resulting in low kinetic Energy on the buckets. As the jet diameter rises, the turbine's total speed lowers. So, the proposed model found that a minimum standoff distance of approximately 40 mm was maintained for each nozzle diameter to reduce the expansion of the jet. Also, it was observed with the Pelton turbine that the significant impact on efficiency was caused by jet misalignment on the turbine and vibrational and frictional losses, reducing the overall efficiency and power developed by the system.
- Compared to the Pelton turbine runner(PTR), the ability to handle the high flow rate of the Turgo turbine has shown increased hydraulic efficiency (η_h) with an increase in the nozzle diameter. A significant improvement in hydraulic efficiency (η_h) was achieved by increasing the overall speed ratio of the turbine under double-nozzle (2n) operation compared to single-nozzle (1n) operation. The maximum power developed from a 10 mm jet diameter, making the jet ratio 11.11 in the Pelton turbine runner (PTR) case.
- The nozzle angle (α) was crucial for testing the runners' hydraulic performance. The normal incidence with a 90° nozzle angle was found more promising compared to deviated other jet angles, 92.5° and 95° in the case of PTR, and TTR is more efficient with a 95° nozzle angle as the jet incidence becomes smoother.
- RSM with central composite design (CCD) effectively optimizes TTR and PTR performance, reducing the need for repeated experiments and facilitating quick design decisions.
- The quadratic model developed by the RSM for the evaluation of hydraulic efficiency (η_h) and the most efficient runner was found to apply to a high degree of accuracy to quantify the hydraulic performance of the runners. The P-value for all the model parameters, such as nozzle angle, nozzle diameter, and number of nozzles at a standoff distance, was below 0.0001, indicating significant effects on the model and, ultimately, the turbine performance. A thorough statistical analysis of the model was conducted to verify its accuracy and validity.
- The optimized conditions for a vertically installed TTR included a 95° nozzle angle, 14 mm nozzle diameter, 40 mm distance from the nozzle tip to the bucket, and double nozzle operation, achieving 66.19% efficiency. The present study revealed that the TTR runner was more sensitive to changes in nozzle angle than the PTR.
- The optimality conditions of the developed RSM model are compared with the results of the experimental investigation to validate the design of geometric parameters. From the validation test, it is found that the error is minimal, which shows that only 0.54 % of actual and predicted values are compared and found with a degree

of agreement. Thus, the validation process has verified the ultimate goal of the study.
- The hydraulic efficiency (η_h) achieved under optimized conditions in the present study is compared with past work, showing good efficiency improvement. The curve follows the trend line up to a 12 mm nozzle diameter, but with a further 2 mm stepped increase in nozzle diameter, the efficiency improves in the case of TTR with a 40 mm nozzle standoff distance.

HIGHLIGHTS

- A Turgo and Pelton turbine Runner with 100 mm PCD in a vertical axis configuration was designed and experimented with.
- The variation in flow, Nozzle diameter (jet diameter,d_j), number of nozzles(n), nozzle angle (jet deviation,α), and nozzle standoff distance ($N_{sod)}$ were kept as independent variables, keeping the head constant.
- The Response Surface Methodology (RSM) with a Central Composite Design (CCD) model was used for the optimization and has shown the effect of each parameter on hydraulic performance.

ABBRIVATION

ANOVA	Analysis of variance
CFD	Computational Fluid Dynamics
RSM	Response Surface Methodology
CCD	Central Composite Design
PCD	Pitch Circle Diameter, mm
PTR	Pelton Turbine Runner
TTR	Turgo Turbine Runner
PLA	Polylactic Acid
1n	Single nozzle
2n	Double nozzle
RANS	Reynolds Averaged Navier-Stokes

Nomenclature

Q	Volumetric flow rate/Discharge, m^3/sec
D_o	The inlet diameter of the nozzle or the inside diameter of the pipe, mm
d_j	Nozzle(jet) diameter, mm
N	Runner speed, rpm
H	Available head, m
N_s	Specific speed
g	Gravitational constant, m/s^2
P_u	Unit power
P_d	Power developed, Watt
P_h	Hydraulic power, Watt
V_{jet}	Velocity of the jet, m/s
u	Peripheral velocity of runners, m/s
T_d	Torque developed at runner shaft, N-mm.
N_{sod}	Nozzle standoff distance, mm
W	Dead weight, kg
S	Spring balance reading, kg

Greek Symbols

ρ	Density of the water, kg/m^3
η_v	Volumetric efficiency,%
α	Nozzle angle, degrees
η_m	Mechanical efficiency,%
η_h	Hydraulic efficiency,%
ϕ_s	Speed ratio/ Velocity ratio
ω	Angular speed, rad/sec
β_2	The jet angle at the bucket exit, degrees
λ_s	Speed or Velocity ratio
ψ_j	Jet ratio

Subscripts

h	Refers to hydraulic
s	Refers to speed
m	Refers to mechanical
2	Refers to exit
j	Refers to jet
sod	Refers to the standoff distance
v	Refers to volumetric
d	Refers to the developed

FUTURE SCOPE OF WORK

The work can be expanded to examine the impact of bucket spacing on performance for runners with a variable bucket number and a greater runner diameter. The bucket's structural analysis can also be studied numerically under dynamic fluid action. The effect of different sustainable materials (compatible with 3-D printing technology) on hydraulic performance can also be explored for further investigation.

ACKNOWLEDGMENT

Thanks to my beloved students, Gaurav P. Bakhru and Darshan N. Modi, for supporting the experimentation and providing help for developing test setup and 3D printed turbine runners at Advance Fluid Mechanics and Fluid Power Laboratory, Sardar Vallabhbhai National Institute of Technology (SV NIT), Surat, Gujarat, India

DISCLOSURE STATEMENT

The authors gratefully acknowledge the TEQIP committee, SV NIT, Suart for funding this study through a core research grant. The sanction order number is TEQIP/phd/2875.

DATA AVAILABILITY STATEMENT

The authors confirm that the data that supports the findings of this study are available within the article. Raw data that support the finding of this study are available from the corresponding author, upon reasonable request.

CONFLICT OF INTEREST

The author declared no potential conflicts of interest with respect to the research, authorship, and/or publication of this article.

ETHICS

There are no ethical issues with the publication of this manuscript.

REFERENCES

[1] Gaiser K, Erickson P, Stroeve P, Delplanque JP. An experimental investigation of design parametcers for pico-hydro Turgo turbines using a response surface methodology. Renew Energy 2016;85:406–418. [CrossRef]

[2] McCarthy MJ, Molloy NA. Review of stability of liquid jets and the influence of nozzle design. Chem Eng J 1974;7:1–20. [CrossRef]

[3] Budiarso, Febriansyah D, Warjito, Adanta D. The effect of wheel and nozzle diameter ratio on the performance of a Turgo turbine with pico scale. Energy Rep 2020;:601–605. [CrossRef]

[4] Alomar OR, Abd HM, Salih MM, Ali FA. Performance analysis of Pelton turbine under different operating conditions: an experimental study. Ain Shams Eng J 2022;13:101684. [CrossRef]

[5] Kholifah N, Setyawan AC, Wijayanto DS, Widiastuti I, Saputro H. Performance of Pelton turbine for hydroelectric generation in varying design parameters. IOP Conf Ser Mater Sci Eng 2018;288:012108. [CrossRef]

[6] Huang F, Mi J, Li D, Wang R. Impinging performance of high-pressure water jets emitting from different nozzle orifice shapes. Geofluids 2020;2020:8831544. [CrossRef]

[7] Gupta V, Prasad V, Khare R. Effect of jet length on the performance of Pelton. Int J Mech Eng Technol 2016;11:11487–11494.

[8] Jung IH, Kim YS, Shin DH, Chung JT, Shin Y. Influence of spear needle eccentricity on jet quality in micro Pelton turbine for power generation. Energy 2019;175:58–65. [CrossRef]

[9] Zhang Z, Casey M. Experimental studies of the jet of a Pelton turbine. Proc Inst Mech Eng A J Power Energy 2007;221:1181–1192. [CrossRef]

[10] Cobb BR, Sharp KV. Impulse (Turgo and Pelton) turbine performance characteristics and their impact on pico-hydro installations. Renew Energy 2013;50:959–964. [CrossRef]

[11] Soe MM, War W, Swe M, Thu AM, Latt AK. Effect of jet angle on the performance of a Turgo turbine. Mandalay (Myanmar): Department of Mechanical Engineering, Mandalay Technological University; 2019.

[12] Catanase A, Barglazan M, Hora C. Numerical simulation of a free jet in Pelton turbine. Proc 6th Int Conf Hydraul Mach Hydrodyn 2004;:6.

[13] Benzon DS, Aggidis GA, Anagnostopoulos JS. Development of the Turgo impulse turbine: past and present. Appl Energy 2016;166:1–8. [CrossRef]

[14] Williamson SJ, Stark BH, Booker JD. Performance of a low-head pico-hydro Turgo turbine. Appl Energy 2013;102:1114–1126. [CrossRef]

[15] Williamson SJ, Stark BH, Booker JD. Low head pico hydro turbine selection using a multi-criteria analysis. Renew Energy 2014;61:43–50. [CrossRef]

[16] Uniyal V, Kanojia N, Pandey K. Design of 5 kW pico hydro power plant using Turgo turbine. Int J Sci Eng Res 2016;7:363–367.

[17] Obayes SA, Qasim MA. Effect of flow parameters on Pelton turbine performance by using different nozzles. Int J Model Optim 2017;7:128–133. [CrossRef]

[18] Safdar I, Sultan S, Raza HA, Umer M, Ali M. Empirical analysis of turbine and generator efficiency of a pico hydro system. Sustain Energy Technol Assess 2020;37:100605. [CrossRef]

[19] Gyanwali S, Kuikel K, Thapa A. Design and CFD analysis of pico hydro Turgo turbine. Proc Int Symp Curr Res Hydraul. Proceedings of the International Symposium on Current Research in Hydraulic Turbines, 2017.

[20] Syofii I, Hidayatullah AB, Adanta D, Sari DP, Burlian F, Saputra MAA. Pico scale Turgo turbine design for remote areas application using velocity triangle approach. J Adv Res Fluid Mech Therm Sci 2022;97:157–167. [CrossRef]

[21] Elgammi M, Hamad AA. A feasibility study of operating a low static pressure head micro Pelton turbine based on water hammer phenomenon. Renew Energy 2022;195:1–16. [CrossRef]

[22] Ishola FA, Kilanko OO, Inegbenebor AO, Sanni TF, Adelakun AA, Adegoke DD. Design and performance analysis of a model pico size Pelton wheel turbine. Int J Civ Eng Technol 2019;10:727–739.

[23] Nigussie T, Engeda A, Dribssa E. Design, modeling, and CFD analysis of a micro hydro Pelton turbine runner: for the case of selected site in Ethiopia. Int J Rotating Mach 2017;2017:3030217. [CrossRef]

[24] Tilahun S, Paramasivam V, Tufa M, Kerebih A, Selvaraj SK. Analytical investigation of Pelton turbine for mini hydro power: for the case of selected site in Ethiopia. Mater Today Proc 2021;:7364–7368. [CrossRef]

[25] Lin TY, Ko CY, Chen SJ, Tsai GC, Tsai HC. A novel total-flow geothermal power generator using Turgo turbine: design and field tests. Renew Energy 2022;186:562–572. [CrossRef]

[26] Oyebode OO. Optimization of the operational conditions for low-head Pelton wheel turbine developed for power generation. J Eng Res Rep 2020;:6–17. [CrossRef]

[27] Hlabanelo JM, Sob PB, Alugongo AA. A study to improve the efficiency and performance of a Pelton wheel using potential energy at low heads. Int J Eng Res Technol 2020;13:2915–2926. [CrossRef]
[28] Lajqi S, Bresa Q, Bresa A, Doçi I, Đurin B. Design, implementation and analysis of the overall performance of a micro hydro Turgo turbine. J Therm Eng 2021;7:806–822. [CrossRef]
[29] Santolin A, Cavazzini G, Ardizzon G, Pavesi G. Numerical investigation of the interaction between jet and bucket in a Pelton turbine. Proc Inst Mech Eng A J Power Energy 2009;223:721–728. [CrossRef]
[30] Xiao Y, Wang Z, Zhang J, Zeng C, Yan Z. Numerical and experimental analysis of the hydraulic performance of a prototype Pelton turbine. Proc Inst Mech Eng A J Power Energy 2014;228:46–55. [CrossRef]
[31] Na S. Simulation of unsteady water film flow on Pelton bucket. Energy Power Eng 2013;5:51–55. [CrossRef]
[32] Xiao YX, Zeng CJ, Zhang J, Yan ZG, Wang ZW. Numerical analysis of the bucket surface roughness effects in Pelton turbine. IOP Conf Ser Mater Sci Eng 2013;52:052032. [CrossRef]
[33] Budiarso, Warjito, Adanta D, Puta NS, Vohra H. Cutout types analysis on pico hydro Pelton turbine. Int J Adv Sci Eng Inf Technol 2018;8:2024–2030. [CrossRef]
[34] Warjito, Budiarso, Siswantoro AI, Adanta D, Kamal M, Dianofitra R. Simple bucket curvature for designing a low-head Turgo turbine for pico hydro application. Int J Technol 2017;8:1239–1247. [CrossRef]
[35] Kim JW, Jo IC, Park JH, Shin Y, Chung JT. Theoretical method of selecting number of buckets for the design and verification of a Pelton turbine. J Hydraul Res 2017;55:695–705. [CrossRef]
[36] Anagnostopoulos JS, Koukouvinis PK, Stamatelos FG, Papantonis DE. Optimal design and experimental validation of a Turgo model hydro turbine. Proc ASME 11th Bienn Conf Eng Syst Des Anal 2012;:157–166. [CrossRef]
[37] Takagi M, Watanabe Y, Ikematsu S, Hayashi T, Fujimoto T, Shimatani Y. 3D-printed Pelton turbine: how to produce effective technology linked with global knowledge. Energy Procedia 2014;:1593–1596. [CrossRef]
[38] Adanta D, Warjito, Febriansyah D, Budiarso. Feasibility analysis of a pico-scale Turgo turbine bucket using coconut shell spoons for electricity generation in remote areas in Indonesia. J Adv Res Fluid Mech Therm Sci 2020;69:85–97. [CrossRef]
[39] Arun K, Kumar KM, Karthikeyan KMB, Mohanasutan S. Analysis on influence of bucket angle of Pelton wheel turbine for its structural integrity using aluminium alloy (A390), austenitic stainless steel (CF20), grey cast iron (325) and martensitic stainless steel (410). Mater Today Proc 2022;:1045–1053. [CrossRef]
[40] Gallego E, Rubio-Clemente A, Pineda J, Velásquez L, Chica E. Experimental analysis on the performance of a pico-hydro Turgo turbine. J King Saud Univ Eng Sci 2021;33:266–275. [CrossRef]
[41] Velásquez L, Posada A, Chica E. Optimization of the basin and inlet channel of a gravitational water vortex hydraulic turbine using the response surface methodology. Renew Energy 2022;187:508–521. [CrossRef]
[42] Betancour J, Romero-Menco F, Velásquez L, Rubio-Clemente A, Chica E. Design and optimization of a runner for a gravitational vortex turbine using the response surface methodology and experimental tests. Renew Energy 2023;210:306–320. [CrossRef]
[43] Guerra J, Velásquez L, Rubio-Clemente A, Jaramillo L, Chica E. Design and optimization of a siphon turbine using the response surface methodology. Results Eng 2024;22:102241. [CrossRef]
[44] Bouvant M, Betancour J, Velásquez L, Rubio-Clemente A, Chica E. Design optimization of an Archimedes screw turbine for hydrokinetic applications using the response surface methodology. Renew Energy 2021;172:941–954. [CrossRef]
[45] Singh U, Gupta NK. Thermal performance analysis of heat pipe using response surface methodology. J Therm Eng 2023;:411–423. [CrossRef]
[46] Gambhir D, Sherwani AF, Arora A, Ashwni. Parametric optimization of blowdown operated double-effect vapour absorption refrigeration system. J Therm Eng 2022;8:78–89. [CrossRef]
[47] Solanki A, Pal Y. Evaluation and optimization of single-effect vapour absorption system for the dairy industry using design of experiment approach. J Therm Eng 2022;8:619–631. [CrossRef]
[48] Ali OM. Spark ignition engine performance analysis with low octane gasoline and methyl tert-butyl ether additive for optimum operation. J Therm Eng 2024;10:911–923. [CrossRef]
[49] Thake J. The micro-hydro Pelton turbine manual. Rugby (UK): Practical Action Publishing; 2000. [CrossRef]
[50] Ebhota WS, Inambao F. Design basics of a small hydro turbine plant for capacity building in Sub-Saharan Africa. Afr J Sci Technol Innov Dev 2016;8:111–120. [CrossRef]
[51] Giosio DR, Henderson AD, Walker JM, Brandner PA, Sargison JE, Gautam P. Design and performance evaluation of a pump-as-turbine micro-hydro test facility with incorporated inlet flow control. Renew Energy 2015;78:1–6. [CrossRef]
[52] Box GEP, Hunter JS, Hunter WG. Statistics for experimenters: design, innovation, and discovery. 2nd ed. Hoboken (NJ): Wiley; 2005.
[53] Raymond MH, Douglas MC, Christine AC. Response surface methodology: process and product optimization using designed experiments. 4th ed. Hoboken (NJ): Wiley; 2016.
[54] Gunaraj V, Murugan N. Application of response surface methodology for predicting weld bead quality in submerged arc welding of pipes. J Mater Process Technol 1999;88:266–275. [CrossRef]

APPENDICES

Appendix A1 Pelton Turbine Runner (PTR) and Turgo Turbine Runner (TTR) Design Specification

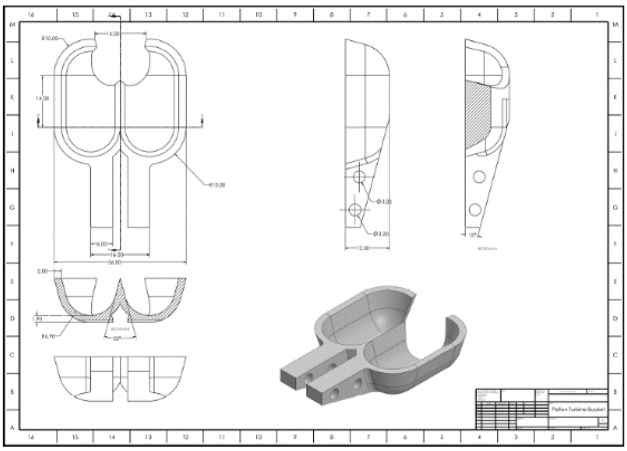

(a) Pelton turbine bucket specification

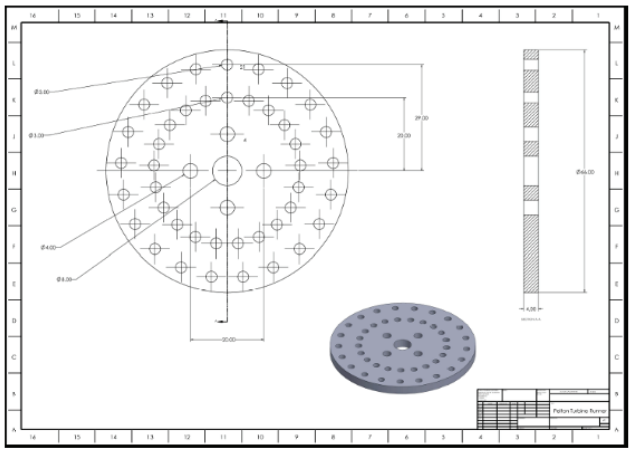

(b) Pelton turbine runner disc specification

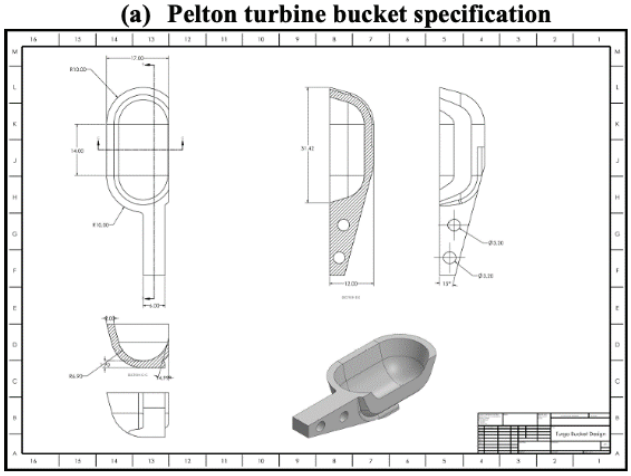

(c) Turgo turbine bucket specification

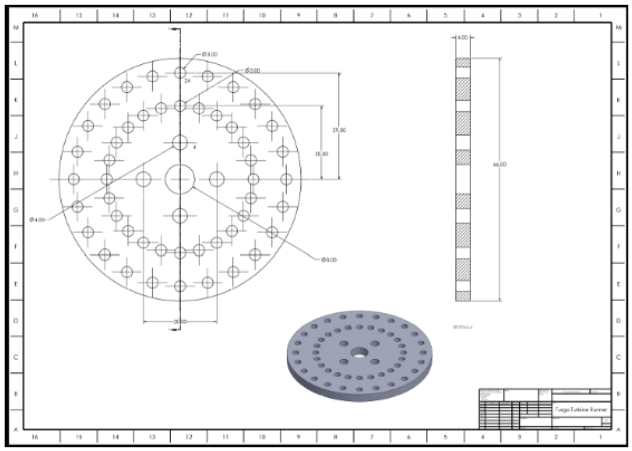

(d) Turgo turbine runner disc specification

Appendix A2: Model summary statistics

Source	Std. Dev.	R^2	Adjusted R^2	Predicted R^2	PRESS	-----
Linear	0.0094	0.8623	0.8530	0.8366	0.0077	-----
2FI	0.0088	0.8956	0.8712	0.8234	0.0084	-----
Quadratic	**0.0053**	**0.9639**	**0.9532**	**0.9375**	**0.0030**	**Suggested**
Cubic	0.0054	0.9743	0.9516	0.8710	0.0061	Aliased

Appendix A3: Fit value for experimental and predicted fit value for experimental and predicted.

Std. Dev.	0.0053	**R^2**	0.9639
Mean	0.6540	**Adjusted R^2**	0.9532
C.V. %	0.8090	**Predicted R^2**	0.9375
PRESS	0.0030	**Adeq Precision**	44.3384

Graphical abstract